Waveguide Enhanced Raman Spectroscopy for Biosensing: A Review

Mohamed A. Ettabib[1,*], Almudena Marti[2], Zhen Liu[1], Bethany M. Bowden[2], Michalis N. Zervas[1], Philip N. Bartlett[2] and James S. Wilkinson[1]

[1]*Zepler Institute for Photonics and Nanoelectronics, University of Southampton, SO17 1BJ, UK*
[2]*School of Chemistry, University of Southampton, SO17 1BJ, UK*
**m.ettabib@soton.ac.uk*

Abstract

Waveguide enhanced Raman spectroscopy (WERS) utilizes simple, robust, high-index contrast dielectric waveguides to generate a strong evanescent field, through which laser light interacts with analytes residing on the surface of the waveguide. It offers a powerful tool for the direct identification and reproducible quantification of biochemical species and an alternative to surface enhanced Raman spectroscopy (SERS) without reliance on fragile noble metal nanostructures. The advent of low cost laser diodes, compact spectrometers and recent progress in material engineering, nanofabrication techniques and software modelling tools have made realising portable and cheap WERS Raman systems with high sensitivity a realistic possibility. This review highlights the latest progress in WERS technology and summarizes recent demonstrations and applications. Following an introduction to the fundamentals of WERS, the theoretical framework that underpins the WERS principles is presented. The main WERS design considerations are then discussed and a review of the available approaches for the modification of waveguide surfaces for the attachment of different biorecognition elements is provided. The review concludes by discussing and contrasting the performance of recent WERS implementations, thereby providing a future roadmap of WERS technology where the key opportunities and challenges are highlighted.

Keywords: Raman sensor, Raman spectroscopy, biosensing, integrated photonics, photonic sensors, waveguide, surface functionalization, WERS, SERS

Demand for low-cost point-of-care clinical diagnostics, environmental detection and pervasive chemical safety and security systems, combined with the advances in standardized silicon-based photonics technologies are enabling rapid growth in biosensing and chemical sensing systems. Chip-based sensing of biochemical species usually exploits the binding of biomolecules in a biological sample to receptors immobilized on the chip surface. Many optical phenomena have been employed to detect this binding and identify and quantify the biochemical species, with refractometry and fluorescent labelling being two of the most successful approaches. In refractometry, the surface density of bound molecules is determined by detecting the refractive index change in a surface layer as the aqueous matrix is displaced by the biomolecules. In fluorescent label-based biosensors, this surface density is most commonly determined by measuring the optical power emitted by the fluorescent-labelled molecules bound at the surface. In both cases specificity is provided by a combination of the surface receptors and an appropriate sample incubation protocol. Refractometry suffers from interferences from non-specific binding (from other biomolecules in the sample) while fluorescent-tagged-based approaches suffer from the cost and inconvenience of labelling and the potential for the label to alter the nature of the binding process. Refractometry is particularly suitable for dynamic measurements of binding, as exemplified by the Biacore Surface Plasmon Resonance (SPR) instrument [1], while photobleaching can render dynamic measurements difficult for

fluorescence-based sensors. Recently, excellent reviews of both approaches have been published [2, 3].

Direct optical spectroscopy of biomolecules offers improved specificity, due to the acquisition of chemically-specific compositional information, and potentially a reduced need for labels or surface receptors. Numerous spectroscopic techniques, such as absorption spectroscopy, fluorescence spectroscopy and Raman spectroscopy, have been utilized to realize significant advances in a wide range of medical, environmental and biological disciplines [4-10]. For instance, fluorescence spectroscopy, using the innate fluorescence of the biological molecules, has been used in detecting cancers [11], diagnosing neurodegenerative diseases [12], studying the microstructural composition of biological tissues [13], and in food processing applications [14]. Similarly, absorption spectroscopy has been utilized in applications ranging from the characterization of catalysts and catalytic reactions [15] and the study of cellular metabolism [16] to remote sensing [17], forensic analysis [18] and detection of air pollutants [19]. Vibrational spectroscopies, such as absorption spectroscopy in the mid-infrared (MIR) part of the spectrum (~2-16 μm) or Raman spectroscopy, offer chemically specific information (or a "fingerprint") at the level of molecular vibrations and are both seeing increased exploitation in biochemical measurements at surfaces. Vibrational spectroscopy serves as a tool to directly identify molecules and their concentrations and vibrational characteristics.

Most untreated biological samples are aqueous and MIR spectroscopy suffers from the strong background absorption of water over much of the MIR. Furthermore, low-cost MIR sources, materials, detectors and spectrometers are at an early stage of development of compared to the near-infrared (NIR ~0.75 - 2 μm) which has benefitted greatly from advances in telecommunications. Nonetheless, significant advances are being made in this field and an excellent perspective on MIR materials and instrumentation for (bio)chemical spectroscopy at waveguide surfaces can be found in Reference [20].

While MIR spectroscopy detects the absorption of radiation at frequencies corresponding to the molecular vibrations, Raman spectroscopy analyses the inelastic scattering of incident photons by the molecules of the sample under test [21, 22]. The scattered photons exhibit a frequency shift relative to the frequency of the incident photons, which is proportional to the vibrational energies of the scattering molecules. In effect, the vibrational frequencies are upshifted by the frequency of the laser "pump" source, translating measurement to a more convenient (visible or NIR) part of the electromagnetic spectrum. This avoids the problems of water absorption but brings the disadvantage of low Raman scattering cross-section (typically 6-8 orders of magnitude lower than fluorescence emission), resulting in the requirement for detection of very low power spectra. Raman spectroscopy and its advanced variants such as coherent Raman scattering [23] and surface enhanced Raman scattering (SERS) [24-27] have been utilized in numerous bio-chemical analysis applications such as the study of viruses and tumors [28, 29], DNA/RNA analysis [30] and monolayer and single molecule detection [31-33]. More details can be found in a number of excellent reviews of various aspects of SERS [34-36] covering both the general field and specific applications.

In SERS the surface enhancement is made up of contributions from a chemical enhancement and from an electromagnetic enhancement. Of the two, the electromagnetic enhancement is the larger contributing a factor of $> 10^4$ as compared to a contribution of typically no more than 10^2 for the chemical enhancement. The chemical enhancement arises when covalent bonding (chemisorption) between the molecule and the metal surface leads to new electronic levels that are close to resonance with the exciting laser light [37] and is highly specific to the particular molecule and metal surface [38]. In contrast, the electromagnetic enhancement [39] arises because of the intensification of the local electromagnetic field at the metal surface and the interaction of this localized electromagnetic

field with the molecules close to the surface; direct bonding to the surface is not essential in this case. The high magnitude of the electromagnetic enhancement arises because there is a contribution from both the light coupling in to the surface wave and a contribution from the light coupling out from the surface [40, 41]. In both cases the enhancement follows the square of the local electromagnetic field and these two enhancement factors combine. Thus a 100 fold enhancement in the in-coupling and out-coupling electric fields at the metal surface will produce an electromagnetic contribution to the Raman intensity enhancement of 10^8. This electromagnetic enhancement decays over a distance of the order 10 – 100 nm, hence the enhancement is surface selective. The orientation of the enhanced electromagnetic field perpendicular to the metal surface has consequences for the specific surface selection rules which, in addition to the general Raman selection rules, determine the intensities of different vibrational bands [42-44]. In SERS those vibrational bands which have contributions from the Raman polarizability tensor component perpendicular to the surface will be the most intense. Consequently, SER spectra are sensitive to the orientation of the molecule. For example, for an aromatic ring standing perpendicular to the metal surface the in plane vibrational modes will be much more intense in the SERS spectrum than the out of plane vibrational modes [45]. In these respects the waveguide enhancement described below is very similar to SERS.

Surface enhanced Raman spectroscopy is an immensely successful approach to identification of biochemical species at low concentration at chip surfaces. SERS chips are normally implemented for use in a conventional confocal Raman spectrometer in place of a conventional microscope slide. This renders the Raman spectrum easily measurable at high speed and SERS is particularly well suited to spectroscopy of molecules at surfaces because of the strong localization of the effect to the metal surface. The principles of operation are well described in the literature [24-27] while recent applications to biochemical measurements are reviewed in [46]. While SERS is suitable for direct Raman “fingerprint” spectroscopy of proteins and DNA, a label (or Raman reporter) is often used, enhancing the limit of detection, providing greater confidence in the species detected, and offering improved potential for multiplexed detection as compared to fluorescence-based techniques [47, 48]. As compared to fluorescence based methods for bio-detection, surface enhanced resonant Raman spectroscopy (SERRS) is an attractive alternative. SERRS measurements are unaffected by quenching, are less sensitive to photobleaching, and are inherently more sensitive. For example, Sabatté *et al.* [49] have shown that the limit of detection for SERRS in an immunoassay application was around one thousand times lower than for the corresponding fluorescence assay. A similar three order of magnitude improvement in the limit of detection was reported by Faulds *et al.* for a DNA assay [50].

However, despite these evident advantages SERS has found limited commercial application to date, probably due to issues with the reproducibility and robustness of the nanostructured metal surfaces. A further significant challenge facing SERS and other spectroscopic approaches to rapid low-cost biochemical detection is in translating the success of these techniques from the research laboratory to point-of-use scenarios [51]. We believe that WERS potentially offers many of the advantages as SERS while at the same time overcoming some of these problems.

Optical waveguide approaches are attractive for sensing and spectroscopy, as the economies of mass-manufacture employed in silicon processing can be exploited, and integrated photonics lends itself to miniaturization, reliable monolithic realization of lab-on-chip configurations on a single substrate and straightforward integration with low-cost lasers, detectors and spectrometers [52-56]. Recently, the use of optical waveguiding to enhance Raman signals at surfaces has re-emerged as a technique with strong potential to address the limitations of SERS [57-62], combining the benefits of integrated photonics with the chemical specificity of Raman spectroscopy. While SERS relies upon complex, narrow-band, lossy resonant metallic nanostructures with low robustness [63-66], waveguide

enhanced Raman spectroscopy (WERS) employs simple, wide-band, nearly lossless robust dielectric waveguides. WERS is based on utilizing the strong evanescent field and long interaction lengths of high-index contrast low-loss optical waveguides to achieve strong excitation of (and collection from) target molecules in the upper-cladding of the waveguide. While for thin, few-moded waveguides the ray analysis of waveguiding is best replaced with a modal analysis [67], a dielectric optical waveguide is, in effect, an extreme, very thin ATR element where the number of "bounces" per unit length is maximized, so that the evanescent power and/or surface intensity is maximized for a given input power. Waveguides fully optimized for surface sensing are ultrathin (~0.1 μm) and support only one mode in each polarization, so that the field distribution and modal velocity is fixed, leading to highly quantifiable operation and great stability. The fabrication techniques employed allow the use of photolithography to readily define the transverse dimension at submicron to mm scales, improving Raman collection efficiency and paving the way for on-chip device integration.

The theory underlying WERS is now well understood and can exploit very well established design tools, used routinely in telecommunications applications, to determine geometries which optimize efficient laser pump – Raman signal conversion and which are readily manufactured using integrated photonics technology.

It is expected that WERS can be used for the same applications as those established for SERS, with modified surface chemistry for dielectric rather than metallic surfaces, and will be competitive if the enhancements can reach comparable levels to SERS. While the levels of enhancements currently achievable by WERS do not match those achievable by SERS, with the continuous advances in nanofabrication techniques and material engineering, waveguide losses are expected to improve, allowing for efficient spiral implementation and resonator structures that facilitate stronger Raman signal build-up. Further advantages of WERS over conventional SERS are that (i) the incident pump light and collected Raman signal need not pass through the sample analyte and (ii) polarization-resolved measurements (e.g. for analysis of molecular orientation) are not constrained to one polarization as they are by the plasmonic nature of SERS. WERS has the potential for greater repeatability and hence improved quantitation, at the expense of longer surface length. Furthermore, WERS promises the realization of low-cost mass-producible microscope-less portable lab-on-a-chip spectroscopic systems that can fill the gap of point-of-use applications.

WERS has also been demonstrated to achieve higher signal-to-noise ratios, and thus better sensitivity, than classic free-space Raman systems both for thin molecular layer sensing and bulk sensing [68]. Despite the higher Raman background signal from the waveguide core, the strong evanescent excitation by WERS sensors results in a stronger Raman signal that builds up along the length of the waveguide. In fact, against confocal Raman microscope systems, WERS have been shown to attain as much as 300 times stronger Raman signal, with a potential theoretical advantage of 2000-fold [69].

In this review, we briefly describe the early realizations of WERS, then discuss the theoretical framework upon which WERS principles are based and review the main resulting design choices for a practical WERS technology. The performance of recent WERS chip implementations is then compared, serving as a basis on which to evaluate design guidelines and highlight the key opportunities and challenges facing WERS technology.

Early Implementations of WERS

Waveguide enhanced Raman spectroscopy was demonstrated as early as 1972 [70] in the form of a 15-25 m long liquid core optical fiber where the Raman spectrum of liquids comprising the core (benzene or tetrachloroethylene) were obtained. Co-propagation of pump and Raman signal along the

length of the fiber allowed the Raman signal to build up, confined within the numerical aperture of the fiber, to achieve strong signals at the fiber output.

Levy *et al*. first demonstrated WERS in a thin-film waveguide in 1974, with the methyl-methacrylate film being studied forming the waveguide guiding layer [71], and pointing out that strong Raman spectra could be obtained from a very small quantity of material using this technique. This again exploited the signal enhancement from confining the pump and signal to co-propagate, building up a strong Raman signal over a 6 mm length of waveguide. In 1979, Rabolt *et al.* continued in this vein showing minimal background Raman from the substrate [72] but then applied thin-film dielectric waveguides to Raman spectroscopy, resonance Raman spectroscopy and orientational studies of monolayers at the surface of waveguides, the monolayers themselves being too thin to support waveguiding [73, 74]. While these studies emphasized that the enhancement was largely due to maintaining high excitation intensity over an increased volume of the material of interest, they did not explicitly address theoretical or experimental waveguide optimization for Raman spectroscopy of surface layers.

In 1996, Kanger *et al*. employed WERS to detection of thin biological films in the evanescent field at a ZnO dielectric slab waveguide surface, demonstrating WERS of a protein monolayer [60]. Theoretical expressions and curves for maximizing the waveguide surface intensity normalized to the waveguided power (and hence the Raman excitation) were given, clearly showing that high index waveguide films (such as ZnO with a refractive index $n \approx 2.0$) offered significantly higher enhancement (~×10) than low-index films (such as glasses with $n \approx 1.53$) and showing that, for this geometry, the enhancement was higher for the TE polarization than the TM. The good signal-to-noise ratio allowed fast acquisition of spectra, enabling dynamic measurements of protein binding, though the authors pointed out that the Raman background from the waveguide film would limit the detectability of weak vibrations, so that other waveguide materials should be sought. Kanger *et al*. then went on to demonstrate stimulated Raman spectroscopy of a thin polystyrene layer on a Si_3N_4 waveguide [75]. With the exception of the liquid core fiber approach [70] and the stimulated Raman demonstration [75], all the WERS demonstrations described above collected the Raman emission from above the surface of the waveguide rather than from its end, and used 1D (slab) confinement rather than 2D (strip or channel) confinement, not fully exploiting the co-propagation and Raman collection potential of WERS.

Theoretical Framework for WERS

Kanger *et al*. [60] made the basic theoretical principles of WERS excitation clear, with subsequent researchers including analysis of waveguide Raman collection and designing and simulating optimized WERS structures. Before considering the recent implementations of WERS which build on this theory, the theoretical foundations of Raman sensing using the evanescent excitation of the target molecule by single mode waveguides are presented, to aid the interpretation of recent results.

The theoretical framework is based on the work of Dhakal *et al*. [76], where the authors present an elegant theory for the excitation and collection of Raman signals using dielectric waveguides. The approach considers an oscillating dipole (modelling the target molecule) at the surface of a dielectric waveguide, as depicted in Fig. 1. An outline description of how the various optical parameters relating to the Raman excitation and collection processes are extracted is presented below.

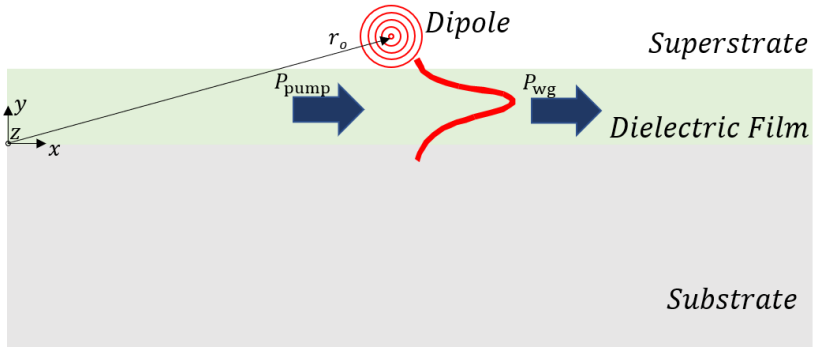

Fig. 1. Schematic diagram of a dielectric waveguide with a dipole, representing the target molecule, at position r_o on its surface. P_{pump} is the waveguide pump power exciting the dipole, while P_{wg} is the power coupled to the waveguide mode from the oscillating dipole after excitation.

Efficiency of evanescent collection of Raman scattering. The emission from a target molecule located at a position r_o in the vicinity of a dielectric waveguide, as shown in Fig. 1, can be modelled as a dipole oscillating at a frequency f = c/λ_o, where c and λ_o are the speed and wavelength of light in vacuum The power coupled to a waveguide mode from the oscillating dipole can then be calculated using Fermi's golden rule as follows [76]:

$$P_{wg}(\vec{r_o}) = P_o \cdot \frac{3n_g}{4\pi n}\left(\frac{\lambda_o}{n}\right)^2 \frac{\varepsilon(\vec{r_o})\left|\hat{d}_o \cdot \vec{\boldsymbol{E}}(\vec{r_o})\right|^2}{\iint \varepsilon_o \varepsilon(\vec{r}) \mid \boldsymbol{E}(\vec{r}) \mid^2 d\vec{r}} \qquad (1)$$

where $P_o = \omega^4 \left|d_o{}^2\right|/(12\pi\varepsilon_o c^3)$ is the power radiated by the oscillating dipole in free space with dipole strength d_o, n_g is the group index of the waveguide mode, n the refractive index at the location of the target molecule, $\varepsilon(\vec{r})$ is the relative permittivity, $\hat{d}_o$ is a unit vector along the dipole, $\omega = 2\pi f$ and $\boldsymbol{E}$ is the electric field strength of the waveguide mode.

Dipole emission with waveguide excitation. Assuming that this dipole is excited via a waveguide mode carrying pump power P_{pump}, travelling in the same waveguide, we can relate the dipole strength to P_{pump} via [76]:

$$|d_o|^2 = a^2 \mid \boldsymbol{E}(\vec{r}) \mid^2 \frac{n_g P_{pump}}{\iint c\varepsilon_o \varepsilon(\vec{r}) \mid \boldsymbol{E}(\vec{r}) \mid^2 d\vec{r}} \qquad (2)$$

where a is the (assumed scalar) polarizability of the dipole. Eqn 2 can be expressed in terms of the Raman scattering cross-section, σ, as follows [77]:

$$|d_o|^2 = \frac{\sigma \lambda^4 \varepsilon_o{}^2}{2\pi^2} \mid \boldsymbol{E}(\vec{r}) \mid^2 \frac{n_g P_{pump}}{\iint c\varepsilon_o \varepsilon(\vec{r}) \mid \boldsymbol{E}(\vec{r}) \mid^2 d\vec{r}} \qquad (3)$$

Combined Raman excitation and collection efficiency. Assuming that the pump and emission wavelengths are close, so that the modal field distributions and group indices are not significantly different, the overall combined Raman excitation and collection efficiency for a single dipole can be described by combining Eqns 1 and 3 to relate $P_{wg}(\vec{r_o})$ to P_{pump} [76]:

$$\frac{P_{wg}(r_o)}{P_{pump}} = \frac{1}{2n}\sigma\lambda^2 \varepsilon_o{}^2 \left(\frac{\mid \boldsymbol{E}(\vec{r}) \mid^2}{\iint \varepsilon_o \varepsilon(\vec{r}) \mid \boldsymbol{E}(\vec{r}) \mid^2 d\vec{r}} n_g\right)^2 \equiv \eta(r_o)\sigma \qquad (4)$$

where $\eta(r_o)$ is the Raman conversion efficiency of the waveguide structure. Clearly, for a specific molecule in a given medium at a fixed position in the evanescent field, the waveguide is optimized by maximizing the product of the 4th power of the normalized electric field strength at that position and the square of the group refractive index of the mode. Note that Kita *et al*. [78] give an analysis for the comparison of different geometries using the separate pump and Raman frequencies explicitly, before making the same assumption that these frequencies were close enough for the waveguide properties to be well enough described using only the pump wavelength in their final expressions, which are similar to [76]. While these expressions give good guidelines for geometrical optimization, it is worthwhile using the electric fields at both wavelengths in numerical simulations, as the pump and Raman wavelengths may easily be separated by 100 nm (~1500 cm^{-1} @ λ_{pump} = 785 nm).

Waveguide length dependence of the Raman signal. In the case of spontaneous Raman scattering and a lossless waveguide, the Raman signal builds up linearly along the length of the waveguide, assuming negligible pump depletion. Figure 2 depicts a waveguide whose upper cladding is uniformly occupied by target scattering molecules with density ρ. Incident pump laser radiation with power P_{in} is coupled to the waveguide via the input facet with a coupling efficiency γ_{in}. The pump is usually coupled into the waveguide either through end-firing or prism coupling [60, 76]. The waveguide pump power at a specific waveguide cross-section, P_{pump}, is related to the incident pump power P_{in} by the coupling efficiency and waveguide loss. The propagating beam excites the scattering molecules, and the resulting scattered spontaneous Raman signal is evanescently collected by the waveguide. Integrating Eqn 4 along the waveguide length using the molecular density and the waveguide losses at the pump and Raman wavelengths yields the total collected power for a bulk analyte. Considering the forward propagating direction, and assuming an output coupling efficiency γ_{out}, the ratio of the collected signal power P_{col} at the end of the waveguide to the incident pump power P_{in} is given by:

$$\frac{P_{\mathrm{col}}(L)}{P_{\mathrm{in}}} = \rho\sigma\eta_{\mathrm{o}}\gamma_{\mathrm{in}}\gamma_{\mathrm{out}}e^{-a_{\mathrm{p}}L}L \qquad (5)$$

where a_{p} is the loss at the pump wavelength and it is assumed for simplicity that the waveguide loss at the pump and Stokes wavelengths is equal; Dhakal *et al.* give the expression when this is not the case [76]. Note that $\eta_{\mathrm{o}} = \iint \eta(r)d\vec{r}$ is the specific conversion efficiency of the waveguide for bulk analytes, which depends on the geometry of the waveguide and can be calculated numerically. The integration is over the entire superstrate cross-section when the system is intended for bulk analyte sensing. However, when the system is designed for sensing a monolayer deposited on the waveguide surface the integration is carried out over only the monolayer. The implication of Eqn 5 is that for maximum conversion efficiency, there is an optimum waveguide length, $L_{opt} = 1/\alpha$, due to decay of both the pump and the collected Raman signal due to loss. Evans *et al.* [79] provide a similar expression to Eqn 5 above with the input and output coupling efficiencies omitted as these are dependent on the coupling method and facet quality and are not intrinsic features of the waveguide itself. Which expression is chosen will depend on whether the chip alone or the whole system is being optimized.

It is important to note that half of the generated Raman signal propagates in the backward (opposite) direction. There are two significant advantages for backward collection: first, the fraction of pump co-propagating with the Raman signal is very small, reducing the extinction required for pump filtering, and secondly, there is no loss-dependent optimum waveguide length unlike the case of forward-collected Raman, where $L_{opt} = 1/a_{\mathrm{p}}$. While loss still limits the achievable Raman signal, the waveguide length does not have to be tailored to the loss and can be made as long as practical to maximise signal. The ratio of P_{col} to P_{in} in the case of backward light collection is given by [80] :

$$\frac{P_{\mathrm{col}}(L)}{P_{\mathrm{in}}} = \rho\sigma\eta_{\mathrm{o}}\gamma_{\mathrm{in}}\gamma_{\mathrm{out}}\frac{1-e^{-2a_{\mathrm{p}}L}}{2a_{\mathrm{p}}} \qquad (6)$$

where it is again assumed that the waveguide loss at the pump and Stokes wavelengths is equal. Note that this efficiency is proportional to $1/a_{\mathrm{p}}$ when L is large, and that lengths L >$2/a_{\mathrm{p}}$ result in less than 2% further increase in signal.

Kita *et al*. [78] have pointed out that the surface intensity and the waveguide loss are usually closely connected, as maximizing the former often maximizes the latter through the effect of surface and sidewall roughness. They perform simulations allowing the Raman signal to be optimized in the presence of modal field dependent excitation, collection *and* loss. These findings will be discussed in the context of recent implementations of WERS in the "Review of Recent WERS Implementations" section.

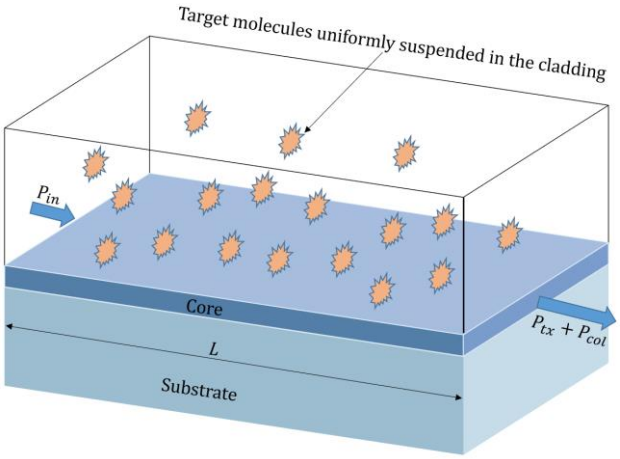

Fig. 2. Diagram of a dielectric waveguide of length *L* whose superstrate is occupied by uniformly distributed molecules.

WERS Design Considerations

In order to exploit the theoretical principles outlined above to realize a WERS sensor with high efficiency and low detection limit, several design choices must be carefully considered. A brief account of the most important of those choices (i) pump wavelength (ii) waveguide materials and (iii) waveguide geometry, is given below:

Pump wavelength

Four key factors affect the choice of pump wavelength for WERS devices, which are (i) the Raman cross-section at the pump wavelength, (ii) the background fluorescence of the waveguide materials and the biological sample at the pump wavelength, (iii) water absorption at the pump wavelength, and (iv) the availability of high-quality low-cost lasers and detectors at the pump wavelength and Stokes wavelengths, respectively.

The Raman cross-section's relationship with wavelength puts a limit on the range of wavelengths that are suitable for a WERS application. This is due to the fact that the cross-section scales as λ^{-4} [81], which means that longer pump wavelengths yield weaker Raman signals. As such, while a standard and mature silicon-on-insulator (SOI) platform operating at 1550 nm offers numerous advantages for on-chip Raman spectroscopy [78] such as CMOS compatibility, low fluorescence and absorption, and the availability of powerful lasers and detectors that are commonly used in telecom applications; the low Raman cross-section of such a platform makes it highly inefficient in comparison with other competing platforms operating at shorter wavelengths.

Conversely, WERS sensors operating at visible wavelengths, such as 532 nm and 633 nm, offer a significantly increased Raman cross-section relative to their mid-IR counterparts. Furthermore, these sensors can utilize pumping close to a molecule's absorption edge (e.g. for hemoglobin in red blood cells) to achieve resonance Raman scattering, and thus an enhanced Raman signal [79]. In addition, low-cost lasers operating at visible wavelengths are commercially available, and the resulting Stokes wavelengths can be detected using high-quality silicon detectors. However, most material platforms, such as silicon nitride (Si_3N_4) [75] and tantalum pentoxide (Ta_2O_5) [82], suffer from increased fluorescence or Raman background when operating in the visible wavelength region, which results in reduced signal-to-noise ratios and poorer detection limits. As such, pumping at the visible wavelength region is restricted to applications involving the detection of molecules with very low auto-fluorescence using waveguide material platforms exhibiting low fluorescence background.

A near-IR wavelength of 785 nm is a popular choice for pump wavelength in biological Raman sensing applications, due to the low water absorption and low fluorescence of biological molecules at this wavelength [83]. In addition, a reasonably high Raman cross-section is still achievable and waveguide materials have reduced fluorescence in comparison with visible wavelengths. However, despite the reduced fluorescence background, there are cases where 785 nm Raman systems are incapable of collecting adequate Raman signals from high fluorescence samples such as lung, liver, and kidney tissues [84, 85]. In such cases, it is often necessary to resort to pumping at longer wavelengths, such as 830 nm and 1064 nm, at the expense of much weaker Raman scattering response [86].

While pumping at even longer wavelengths is uncommon due to the significant reduction in the already weak Raman cross-section, the use of silicon-on-insulator (SOI) platform, which requires pumping above the silicon bandgap of 1.14 eV (1088 nm), is an alternative that has nevertheless been considered [87] due to the platform's very high refractive index and high maturity, which spans decades of research and development, resulting in the ability to make highly complex waveguide structures and lab-on-chip devices with high efficiency and repeatability and very low losses. The high refractive index allows the platform to achieve a stronger evanescent field for the pump-analyte interaction, which acts to compensate the performance reduction due to the reduced Raman cross-section. However, pumping at these longer wavelengths means that the commonly used efficient silicon-based CCD detectors cannot be used, since their quantum efficiency starts to roll off at wavelengths beyond 1 μm. In addition, the use of silicon waveguides means that there is a limit on the amount of pump power that can be used due to nonlinear two-photon absorption.

Waveguide materials

Selecting a suitable material for a WERS sensor involves several considerations, such as the value of the material's refractive index, its transparency window, its background Raman and fluorescence responses at the pump and Stokes wavelengths, and the ease of fabrication.

An ideal WERS sensor should be made from a material with a high refractive index, since such a material can be used to realize a waveguide with a high index contrast, where a strong optical confinement can be achieved, leading to an increased evanescent field intensity by which to probe the target analyte. The material should exhibit low absorption at the visible and near infrared wavelengths, and yield waveguides with low surface scattering, thus allowing the Raman signal to build up along the interaction length. In addition, the material should offer low background emission at the Stokes wavelengths of interest. The material background includes its Raman and fluorescence background emission, as well as fundamental thermodynamic fluctuations, which all impact the signal-to-noise ratio of the system. While the Raman and fluorescence background responses have been well-studied and are typically dominant at smaller Raman shifts, the importance of thermodynamic

fluctuations have only recently been highlighted [80, 88]. These thermodynamic fluctuations result in background noise in the optical spectrum which becomes dominant at larger Raman shifts.

In a recent paper [89], four of the most commonly used photonic platforms for WERS applications have been experimentally compared in terms of their broadband background emission and their Raman conversion efficiency at a pump wavelength of 785 nm. The platforms compared were aluminum oxide (Al_2O_3), silicon nitride (Si_3N_4), tantalum pentoxide (Ta_2O_5) and titanium dioxide (TiO_2). Rib waveguides were fabricated from each material, where the waveguide geometry was engineered to support the TE fundamental mode at the pump and signal wavelength, achieve low loss and realize a high specific conversion efficiency (η_O). Table 1 lists the values of the measured loss and calculated Raman collection efficiencies for the four waveguide platforms [89]. In this table, η_A corresponds to the analyte Raman conversion efficiency while η_{BG} corresponds to the conversion efficiency for Raman background originating from the waveguide materials.

Table 1. comparison of the refractive index, waveguide geometry, loss and Raman collection efficiencies for the four waveguide platforms used in the study reported in [89]. Reprinted with permission from [89] The Optical Society.

material	refractive index (n_c)	waveguide geometry (w×h) nm^2	loss, α_m (dB/cm)	η_A	η_{BG}
Al_2O_3	1.60	900 × 450	1.9–2.6	0.013	0.27
Si_3N_4	1.89	700 × 220	2.0–3.1	0.053	0.49
Ta_2O_5	2.11	500 × 220	4.8–5.4	0.13	0.61
TiO_2	2.33	380 × 180	7.0–8.0	0.18	0.79

Figure 3 shows the measured emission spectra for all four platforms with no analyte (i.e. air cladding). The spectra show that TiO_2 has significantly stronger background emission than the other three platforms (the TiO_2 spectrum in Fig. 3 is scaled down by a factor of 8 for display purposes).
Al_2O_3 exhibits the weakest scattering background, while Ta_2O_5 has a relatively low scattering background at most wavelengths, with a Raman peak occurring at 660 cm^{-1} due to Ta-O stretching vibrations of TaO_6 octahedra [90]. Finally, the background emission of Si_3N_4 is higher at shorter wavelengths, but rapidly decreases with wavelength.

Shot noise associated with the background emission is the ultimate limiting factor in the signal-to-noise ratio and hence limit of detection for WERS [91], so that optimization should consider maximization of the ratio of Raman signal power to background power falling on the detector. Dhakal *et al*. [91] have shown that the background in the case of Si_3N_4 waveguides is primarily due to Raman emission rather than fluorescence, and that the Raman emission from the SiO_2 substrate is small compared with that from the Si_3N_4 core.

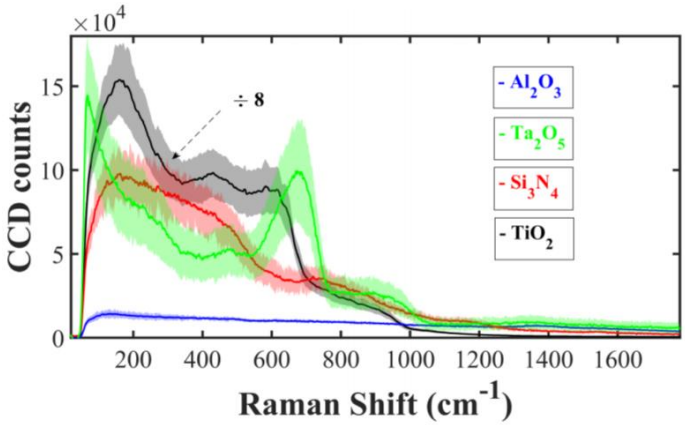

Fig. 3 Background scattering spectra for the four material platforms studied in [89], normalized by length factor and coupling efficiency. Reprinted with permission from [89] The Optical Society.

To put the significance of this scattering background data into perspective, the authors used waveguides from Al_2O_3, Si_3N_4 and Ta_2O_5 to measure the Raman spectrum of ethanol. A comparison of the strength of the detected Raman mode of ethanol at 880 cm^{-1} by the three material platforms showed that Ta_2O_5 collected the strongest Raman signal followed by Si_3N_4 and then Al_2O_3, in agreement with the trend of the specific conversion efficiency in Table 1. A further study comparing Al_2O_3, TiO_2 and Si_3N_4 waveguides for WERS of toluene in terms of signal and background has subsequently been published [92] drawing similar conclusions for these three materials, but differences in waveguide geometry and loss make firm conclusions elusive.

While it may be tempting to dismiss the usefulness of the TiO_2 platform for Raman sensing applications, one must bear in mind that the high scattering background reported in [89] may be a by-product of the fabrication parameters used in the study. Indeed, this assumption is supported by the fact that a significantly lower scattering background was reported in [79] for TiO_2 waveguides fabricated by sputtering. In addition, a platform such as TiO_2 may in fact excel (and outperform other alternatives) in visible-wavelengths (rather than at a near-IR wavelength of 785 nm) evanescent Raman sensing applications to analyze materials without auto-fluorescence. This is due to the chemical stability, biocompatibility and low fluorescence of TiO_2, which make it a suitable platform for sensing a wide range of chemical and biological agents [79].

Pope *et al.* [93] have used chalcogenide glass films of As_2S_3 on SiO_2 substrates for WERS and show the waveguide Raman emission (background) spectrum to be limited to below 500 cm^{-1}. The refractive index of this material at 785 nm is ~ 2.45, offering potential for high Raman conversion efficiency due to high index contrast, but experimental differences make direct comparisons difficult.

While Si_3N_4 offers good performance and has the great advantage of using well-established silicon-based fabrication processes, improvements in materials and fabrication techniques to reduce background emission and waveguide loss may lead to other materials systems prevailing. Further, while the impact of the thermodynamic fluctuations on the sensitivity and detection limit of amorphous waveguides has been recently established, crystalline media are yet to be investigated. The use of crystalline waveguides may result in resonantly enhancing the background in some frequency bands due to scattering via polariton modes while reducing the broadband background, and therefore may yield improved signal to background ratios in the detection of specific analytes [80].

Waveguide design

The waveguide design process for WERS generally involves two key stages, namely, selecting the waveguide type (i.e. geometry) to be used, and choosing the structural parameters (i.e. dimensions) for the selected waveguide type.

There are several waveguide geometries that can be used for a WERS sensor, with slab (planar) [60], strip [79] and slot waveguides [87] being the most commonly used. Figure 4 depicts these three types along with mode profiles for an SiO_2-Si_3N_4-Air system at 785nm with some typical structural geometries.

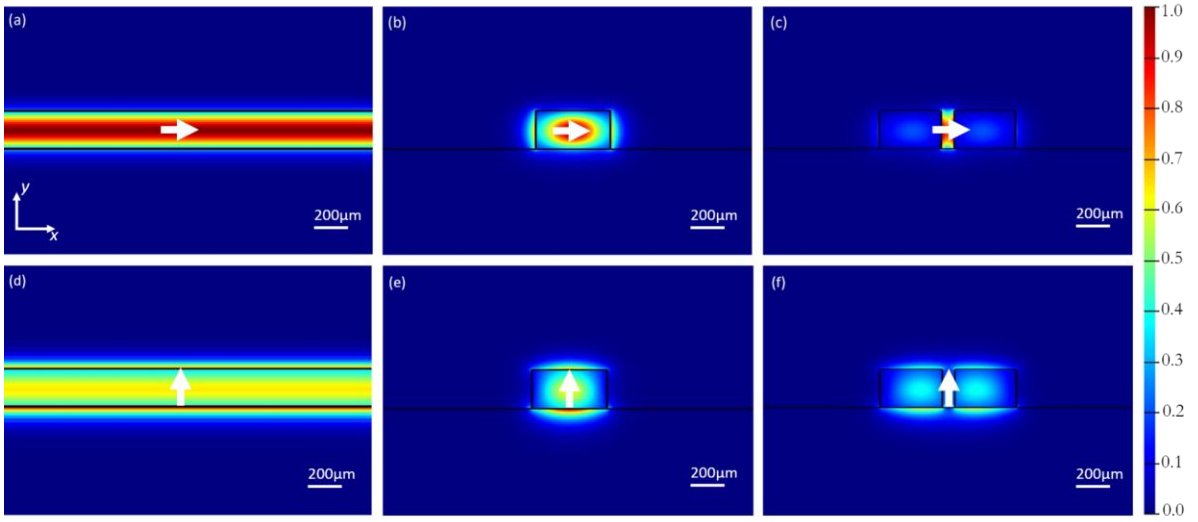

Fig. 4. Waveguide cross-section overlaid with the simulated fundamental modal intensity distribution for (a,d) slab, (b,e) strip and (c,f) slot waveguides for TE (top) and TM (bottom) polarizations. The slab waveguide exhibits pure TE and TM modes, while the strip and slot waveguides exhibit quasi-TE and quasi-TM modes. The arrows indicate the major E-field direction.

The slab geometry (Fig. 4(a) and (d)) is the simplest, and the pump can interact with a large area of the analyte. However, maximizing the illuminated width does not yield an advantage, as while more molecules are probed as a result, each experiences a proportionally reduced pump intensity. It is therefore the length of the waveguide that is most significant, as the Raman signal can build up along the waveguide length. Maximizing the length of slab waveguides is limited to the length of the chip, which should be short for compactness and cost, and such waveguides are therefore limited to a few cm in length. The design of slab waveguides simply involves choosing the waveguide thickness to maximize the square of the magnitude of the electric field at the surface. Kanger *et al*. [60] first presented the waveguide surface intensity normalized to the modal power per unit width of the waveguide, as a means to optimize Raman excitation (of for example a monolayer) at a waveguide surface. Dhakal *et al*. makes clear, however, that optimization of both excitation and collection should be in terms of the square of the magnitude of the electric field, $|E|^2$, as in Eqn 4, rather than in terms of the intensity, as the former is proportional to the local energy density, because in the TM case, intensity takes into account only one component of the electric field [94]. Figure 5(a) plots the surface intensity, and Fig. 5(c) shows $|E|^2$, for the fundamental TE and TM modes of a Ta_2O_5 slab waveguide on an SiO_2 substrate, with an air superstrate, at 785 nm, and with the mode carrying 1 W power per meter slab width. The figure shows that there is an optimum core thickness at which the maximum surface intensity, and $|E|^2$, is achieved. Thicker films result in a stronger mode confinement in the core, and therefore a reduced evanescent field and surface intensity. Films thinner than the optimum thickness have a larger portion of the evanescent field in the substrate, and therefore poorer mode guidance in the core and a lower surface intensity. Comparing, Figs. 5(a) and 5(c) it is clear that the TM polarization yields the stronger Raman excitation.

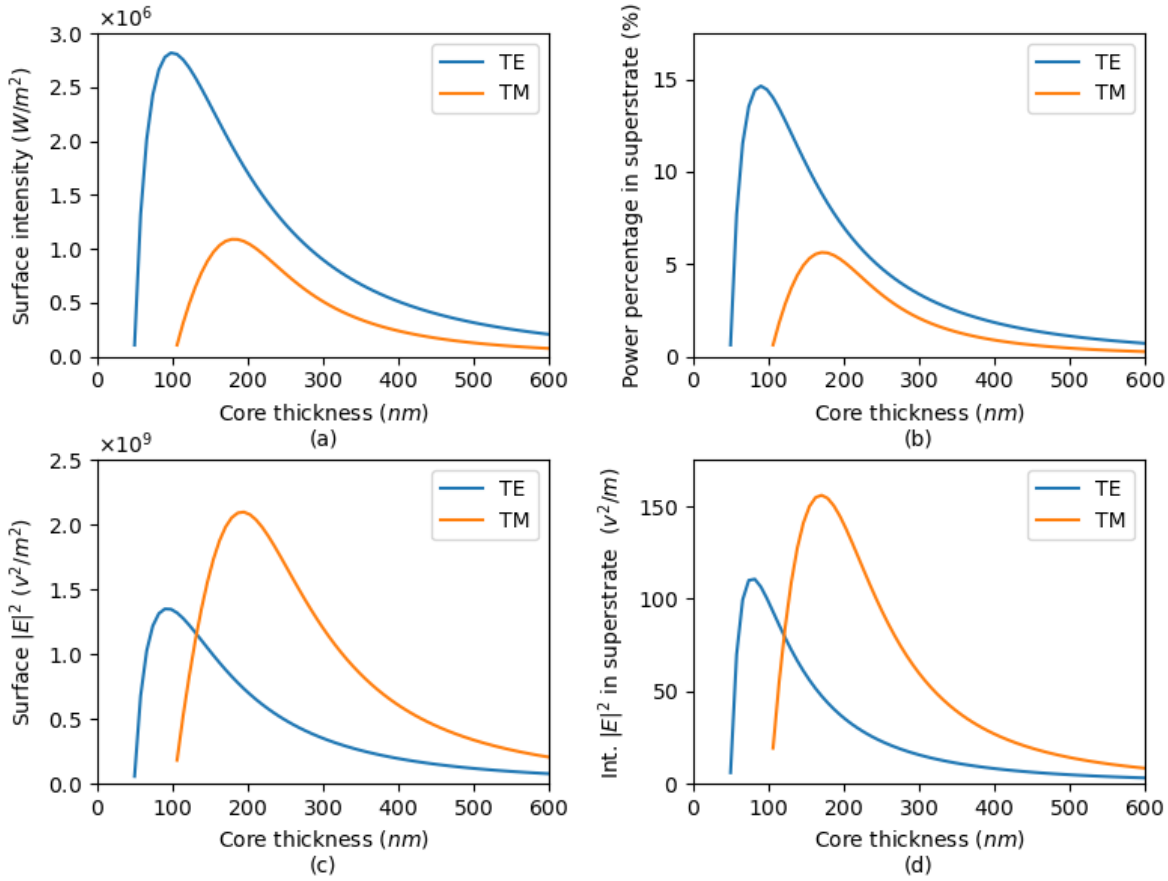

Fig. 5. (a) Normalised surface intensity (b) percentage superstrate power (c) surface $|E|^2$, and (d) $|E|^2$ integrated over the superstrate, for the fundamental TE and TM mode of a Ta_2O_5 waveguide as a function of film thickness at 785nm. The mode carries 1W power per metre waveguide width.

While WERS offers greater advantages for spectroscopy of thin surface films, many measurements of bulk analytes have been made. Fig. 5(b) and (d) show the power fraction in the superstrate and $|E|^2$ integrated over the substrate, the latter being used to optimize for analysis of bulk analytes.

In common with slab waveguides, the design of strip and slot waveguides for WERS must take into account the effects of waveguide dimensions and refractive indices on the efficiency of the Raman scattering process, optimizing the modal electric field in the analyte medium. Dhakal *et al.* have described the design process in detail [87], numerically optimizing the specific conversion efficiency of the waveguide η_0 described in the previous section (which is a function of the electromagnetic conditions and the geometry of the waveguide alone) in order to optimize the Raman conversion efficiency.

Strip waveguides (Fig. 4(b) & (e)) differ from slab waveguides by lateral light waveguiding in the film plane, providing guidance in two dimensions, rather than just one. There are two potential advantages of strip waveguides for WERS: (i) they guide all the light collected along the waveguide to its end and (ii) they allow much longer interaction lengths in a small chip area, through the implementation of spirals [76]. However, the latter advantage is only realizable if the waveguide propagation loss is low, as the loss-dependent optimum length ($L_{opt} = 1/\alpha$) is less than 2.3 cm in all the waveguides reported in Table 1.

Slot waveguides, on the other hand, feature two high refractive index strips that are placed adjacent to a lower refractive index slot (Fig. 4(c) & (f)). The width and aspect ratio of the two strips, along with the width of the slot can be engineered to provide various modal confinement properties. In the

context of WERS applications, they are often engineered to provide strong light enhancement in the slotted region of the waveguide, thereby resulting in lower background Raman and fluorescence emission (but not necessarily lower thermodynamic fluctuations) from the waveguide material, and stronger interaction with the analyte, although there may be mass transport limitations in analytical applications with very narrow slots. As such, they can provide superior signal-to-noise ratios, though slot waveguides present increased input power launching challenges.

Both strip and slot waveguides require additional lithographic and etching steps to realize lateral confinement, and the resultant side-wall roughness normally increases waveguide losses, and therefore the useful lengths of the waveguides and thus Raman signal. However, with continuous improvement in nanofabrication and post-processing techniques, one can envisage that such challenges will be eased, allowing for much more efficient waveguides than those currently technologically achievable.

Overall, WERS design considerations concerning wavelength, material, waveguide structure and polarization are so dependent on less well controlled parameters such as waveguide loss and material background that no clear leading approach has yet emerged. However, the most promising approaches are further elucidated in the discussion of present WERS implementations in the penultimate section of this review.

Surface Biofunctionalization for WERS

WERS relies on the electromagnetic enhancement at the waveguide surface to enhance the Raman intensity, in much the same way as the enhancement in SERS, and therefore has high sensitivity for species at the waveguide surface. Point-of-care medical diagnostics typically requires the detection of specific biomarkers [95] at very low concentration (aM levels) [96-98] in complex matrices (blood, urine, etc.) with minimal sample pretreatment. To utilize the surface sensitivity and the surface enhancement offered by WERS in these applications it is necessary selectively concentrate the desired biomarker(s) at the waveguide surface and this can be achieved by immobilizing suitable biorecognition elements (antibody, enzyme, DNA, etc.) at the waveguide surface. In this respect WERS is similar to SERS and surface plasmon resonance (SPR). Chemical surface modification is, therefore, an important element in the design of these types of biosensor. In this section, we briefly review the available approaches for the modification of waveguide surfaces for the attachment of different biorecognition elements. There are many well established tried and tested methods for immobilizing biorecognition elements at surface and many suitable commercial sources of biorecognition elements designed for surface attachment. We therefore begin by considering these established approaches before going on to consider how to modify the surface of a waveguide to be compatible with them.

Chemical surface modification

The most commonly used biorecognition elements are antibodies, nucleic acids, cell membrane receptors, peptides, and enzymes. These biomolecules show extraordinary affinity and specificity towards particular analytes, allowing the selective capture of the target at low target concentration. The selection of the appropriate protocol to immobilize the biorecognition element onto the surface is an important consideration in biosensor design. The material used to fabricate the waveguide and the reactive functional groups available on the biorecognition element dictate the choice, or choices, of immobilization chemistry.

For effective use, immobilization should be efficient and give good, reproducible and stable surface coverage, without significantly degrading the recognition properties of the biorecognition element or the sensitivity of the transducer [99, 100]. The simplest way to immobilize the biorecognition molecule on the sensor surface is by physical adsorption based on electrostatic, hydrophobic and polar

interactions between the biomolecule and the surface. The disadvantages of this simple approach are that there can be distortion of the biomolecule at the surface affecting its binding to the analyte; desorption of the biomolecule can occur due to changes in the pH or buffer composition in flow assays; and the orientation of the adsorbed biomolecule is not necessarily reproducible or well controlled [101]. A better approach is to deliberately functionalize the surface. This is usually achieved by chemically modifying the surface with a bifunctional linker molecule in which one end reacts with the surface and the other end can be coupled to the biorecognition element. In some cases, these bifunctional linkers can be used to produce self-assembled monolayers (SAMs) with well-defined packing and density of the molecules at the surface [102, 103]. In general the terminal functional group is used to covalently link molecules to the surface using well established chemistries (for example by forming an amide or ester) or by using non-covalent interactions with high affinity species (such as biotin-streptavidin, or the use of cofactors or site-directed affinity proteins [104]).

No matter how the biorecognition element is attached to the sensor surface non-specific adsorption is always a complication for real world applications. The most convenient way to minimize such non-specific signals is to design bioreceptor surfaces able to suppress the fouling by unspecific molecules. There is no universal method to suppress non-specific binding and the chosen blocking method will depend on the complexity of the analysis sample; for example blood and serum present the biggest challenge. Part of this design may require the immobilization of specific groups at the sensor surface along with the biorecognition element.

Schemes 1 and 2 summarize common chemistries used to immobilize biomolecules at surfaces. Accessible amine groups naturally present, or deliberately introduced, in the biorecognition element are frequently used and can be covalently linked to different surface functional groups including amine ($-NH_2$), carboxylate (-COOH), hydroxyl (-OH), thiol (-SH) or epoxy (-OR) groups (Scheme 1) [100]. Alternatively thiol groups on the biorecognition element can be used to attach the molecule to a variety of surface functional groups, Scheme 2, using an appropriate coupling reagent [105]. Water-soluble crosslinkers (sulfonate analogues) are often favored as they give consistently higher coupling yields than their insoluble counterparts [106].

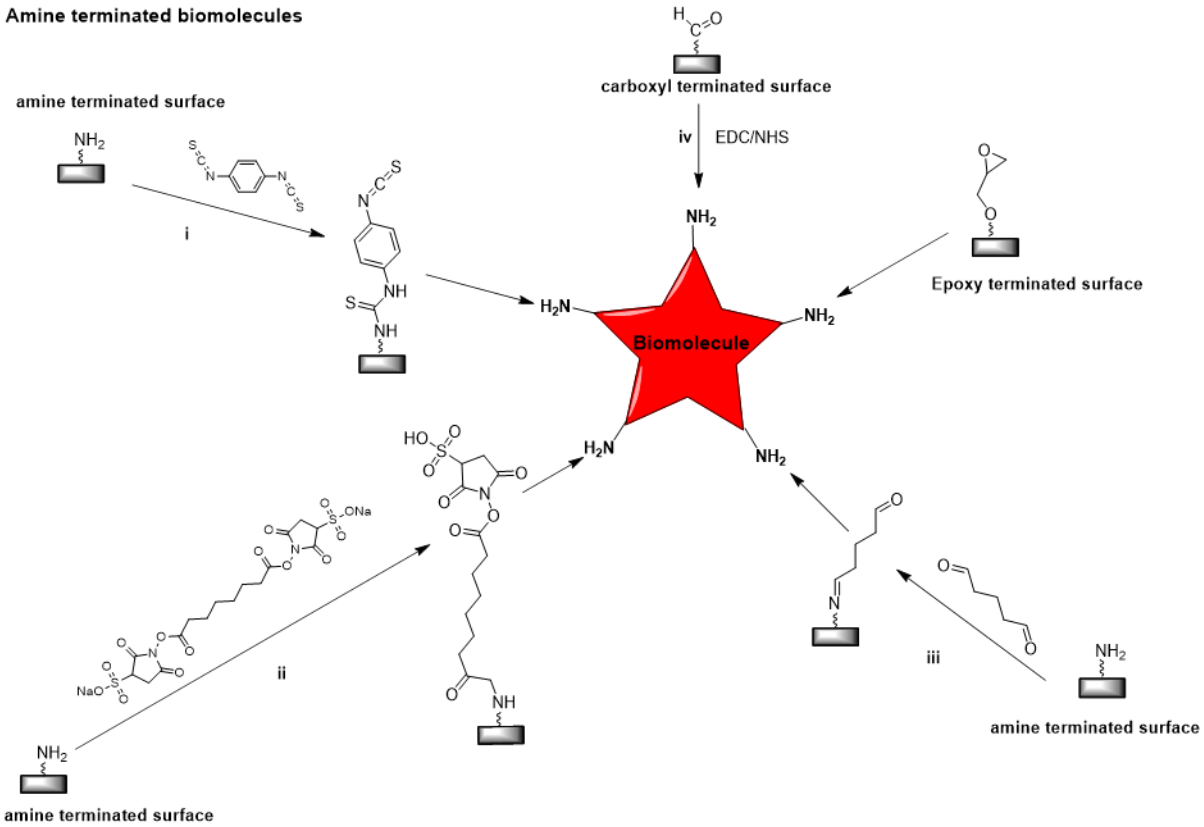

Scheme 1: The common strategies to immobilize amine labelled biomolecules onto surfaces. i) PDITC: p-phenylene diisithiocyanate; ii) BS3: bissulfosuccinimidyl suberate; iii) Glutaraldehyde; iv) EDC/NHS: 1-ethyl-3[3-dimethyl-nopropyl]-carbodiimide/N-hydroxysuccinimide.

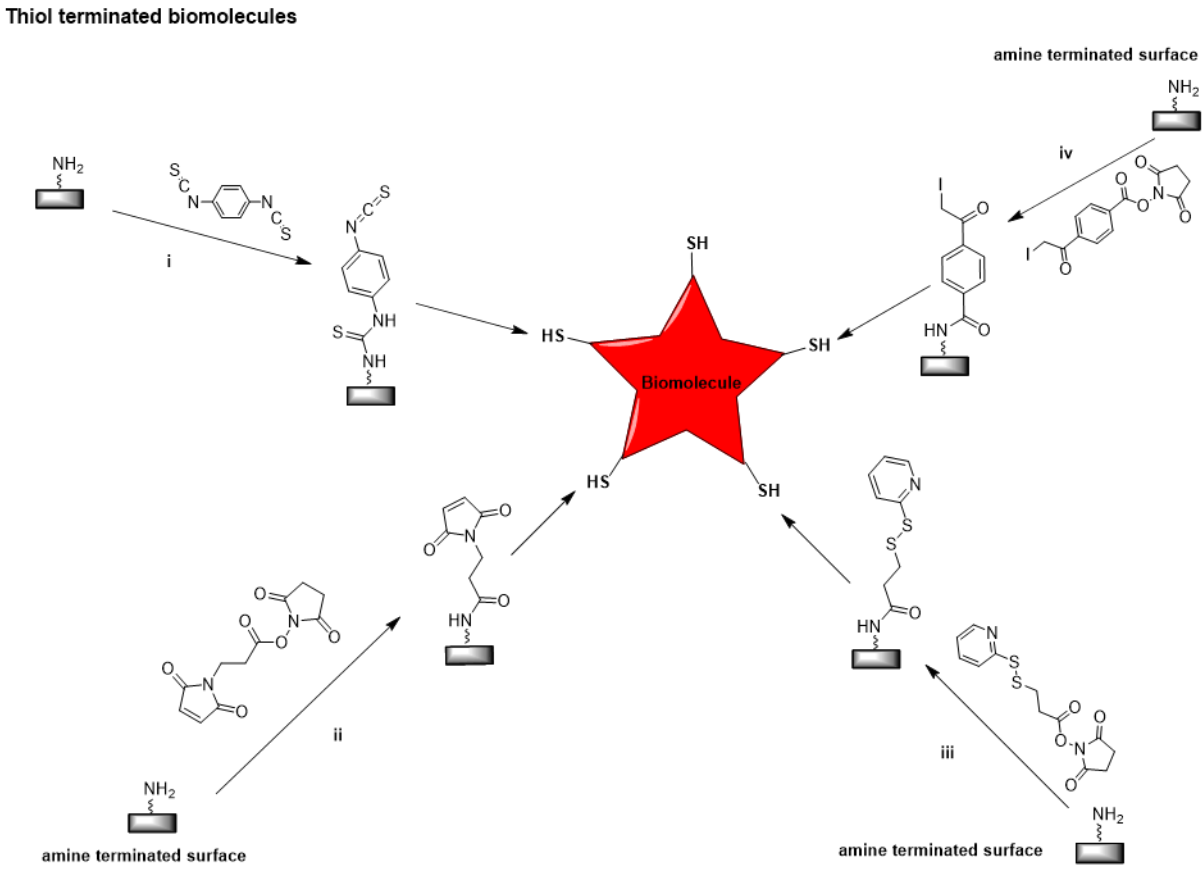

Scheme 2: The common strategies to immobilize thiol labelled biomolecules onto surfaces. i) PDITC: 1,4-phenylene diisothiocyanate; ii) SMP: N-succinimidyl-3-maleimidopropionate; iii) SPDP: N-succinimidyl-3-(2-pyridyldithio) propionate; iv) SIAB: N-succinimidyl (4-iodoacetyl) aminobenzoate [118].

The most common chemistry used to covalently bind amino-terminated biomolecules to modified surfaces is based on N-hydroxysuccinimide (NHS) esters (Scheme 1) which can react with primary and secondary amines to create stable amide (-NH-CO-) and imide (-CO-NH-CO-) linkages [107, 108]. Carboxylate-terminated surfaces can be functionalized with amine-functionalized biomolecules after reaction of the carboxylic acid and N-hydroxysuccinimide (NHS) in the presence of N-ethyl-N'-(3-dimethylaminopropyl)carbodiimide (EDC) [109]. The preferred crosslinker to activate amino-modified substrates with isothiocyanate functional groups (Scheme 1i) is *p*-phenylene diisothiocyanate (PDITC). PDITC has the potential to form well organized assemblies driven by π–π stacking, significantly decreasing non-specific binding [110].

Although glutaraldehyde (Scheme 1iii) has been widely used as a crosslinker between amino-terminated substrates and biomolecules [111] it has some undesirable effects, such as the formation of multilayers [112]. Amino-terminated surfaces also permit the attachment of thiol terminated biomolecules using the hetero-bifunctional crosslinker N-succinimidyl-3-maleimidopropionate (SMP) [113] (Scheme 2ii). The use of disulfide bonds, such as N-succinimidyl-3-(2-pyridyldithio) propionate (SPDP), offers the advantage of surface regeneration for repeated biosensing measurements [114]. Epoxy chemistry is an alternative coupling approach for biomolecule immobilization given its stability under aqueous conditions and its reactivity to several nucleophiles; it can be used to conjugate thiol, amine, or hydroxyl terminated biomolecules [115, 116]. However, the reaction of amines with epoxides requires the reaction medium to be at high ionic strength, which can cause denaturation of proteins [117].

Fortunately there are many commercial labelling kits for antibodies, enzymes, proteins and DNA available based on bioconjugation techniques, such as amino reactive molecules using crosslinking or biotinylated reagents [118, 119]. which provide a simple route to the bioconjugation provided that the appropriate reactive functional group can be introduced at the waveguide surface.

Chemical modification of the waveguide surface

As has been discussed in the previous subsection, there are several well-established methods for attaching biological molecules to functional groups (-NH_2, SH, CO_2H, etc.) presented on a surface. Thus to attach the biorecognition element to the waveguide surface one first needs to chemically modify that surface. The ways in which this can be achieved depends on the particular waveguide material. To date, most studies using WERS have been performed using silicon nitride (Si_3N_4) [100]. In addition, there are other possible materials such as alumina (Al_2O_3), titanium dioxide (TiO_2) or tantalum pentoxide (Ta_2O_5) that have been shown to be suitable [89]. We will therefore review the methods available to chemically modify these different surfaces. Clearly the first step is to find ways to attach species to the surface.

Silanization of metal oxides. To date the most common approaches for the chemical modification of WERS waveguide make use of well-established methods for attaching molecules (grafting) to silica surfaces, mainly using organosilanes [100, 120]. This chemistry can be extended to the surfaces of other metal oxides, e.g. Al_2O_3 [121], TiO_2 [122] or Ta_2O_5 [123] as shown in Scheme 3a.

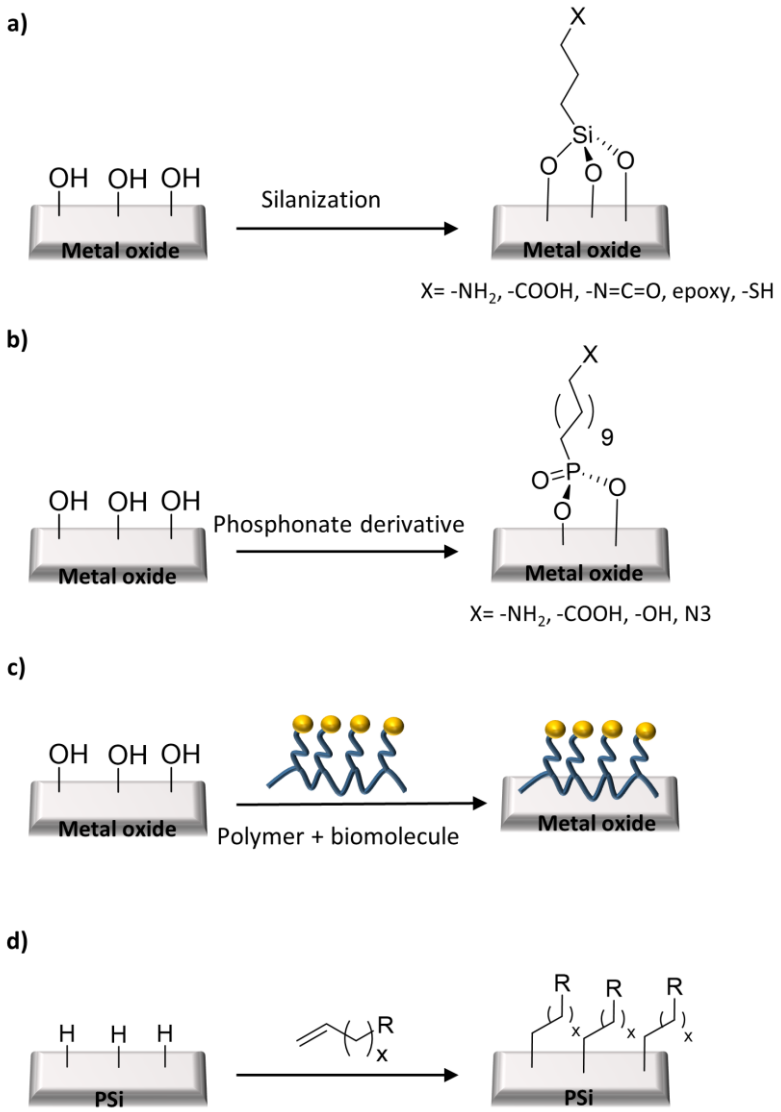

Scheme 3: Surface coupling chemistries for activated oxide or hydrogen terminated Si surfaces [124].

In general, the oxide surface needs to be cleaned and treated to maximize the number of surface -OH groups. The most common approaches to do this are to use oxygen plasma, piranha solution, or UV/O_3 treatment. These all make the surface hydrophilic.

A typical example of silanization can be found in the work of the Swanson group who described a waveguide biosensor for the detection of tumor and infectious disease biomarkers based on a sandwich immunoassay using SAMs or lipid bilayers [125-128]. The waveguides were made from $SiON_x$ modified with a thin layer of SiO_2. The SiO_2 was functionalized using an amine-terminated organosilane and the resulting amine-terminated surface was then covalently linked to biotin using N-hydroxysuccinimide (NHS) ester functionalization. The biotin was then used to attach streptavidin-modified antibodies to the surface utilizing the strong affinity binding between biotin and streptavidin [127]. Figure 6 shows the configuration where the surface-O-Si bonds bind the silane molecules to the surface and where flexible polyethylene glycol (PEG) chains are used both to suppress non-specific binding and to attach the biotin (the R group in the Figure 6).

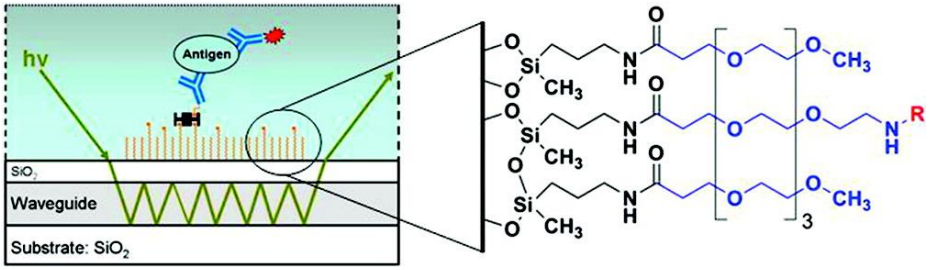

Fig. 6. Waveguide biosensor for the detection of tumor biomarkers based on a sandwich immunoassay. The amine-terminated films were chemically modified with a mixture of carboxylic acid-terminated poly(ethylene glycol) (PEG) chains, in blue, of varying functionality. A fraction of the PEG chains terminated in biotin (R), which produced a surface with an affinity toward streptavidin [128]. [Reprinted (adapted) with permission from [128]. Copyright (2021) American Chemical Society]

Kozma *et al*. [129] reported a label free waveguide biosensor based on Ta_2O_5, where the waveguide surface was modified with an amino-terminated silane followed by functionalization with avidin by glutaraldehyde crosslinking. Xin and co-workers [130] designed a waveguide surface for the detection of *E. coli* in which the surface of the SU-8 waveguide was activated by oxygen plasma and then modified with an amino terminated silane. They then used glutaraldehyde as a crosslinker for the immobilization of the antibodies.

Silanization is popular because it is relatively easy to carry out and the silane reagents are readily available, however the formation of a reproducible and well-defined monolayer is exceedingly difficult. The major problem is the propensity of the system to form multilayers because of cross condensation of the silanes to form Si-O-Si linkages [103].

Modification of metal oxide surfaces with organophosphonate derivatives. Although silanization is the most widely adopted approach in the literature the use of phosphonates ($-PO(OH)_2$) for attachment to metal oxide surfaces (Scheme 3b) is growing due to the fact that phosphonate derivatives are less predisposed to self-condensation [131]. In addition, phosphonates form more stable and better ordered monolayers. Compared to silane SAMs, organophosphonate derived SAMs are more resistant to hydrolysis under physiological conditions and do not require pre-treatment of the surface with acid to obtain high coverage. Phosphonate SAMs show excellent biocompatibility and chemical resistance to humid conditions making them well suited to use in biological fluids [131].

The work of Canepa *et al.* [132] provides an example of this approach. They describe the use of an amine terminated phosphonate to form monolayers on TiO_2 which were then used to develop a further functionalization with antimicrobial peptides. Muriano and co-workers [133] reported an immunosensor assay based on a Ta_2O_5 waveguide where the surface was modified with phosphonohexanoic acid followed by covalent coupling of antibodies as a methodology for immobilization of the biorecognition molecules, Figure 7. In another example, phosphonic acid derivatives were used to functionalize TiO_2 surfaces with thiol-terminated SAMs for further modification with proteins. This strategy provides an approach for biomolecule immobilization and patterning onto TiO_2 surfaces [134].

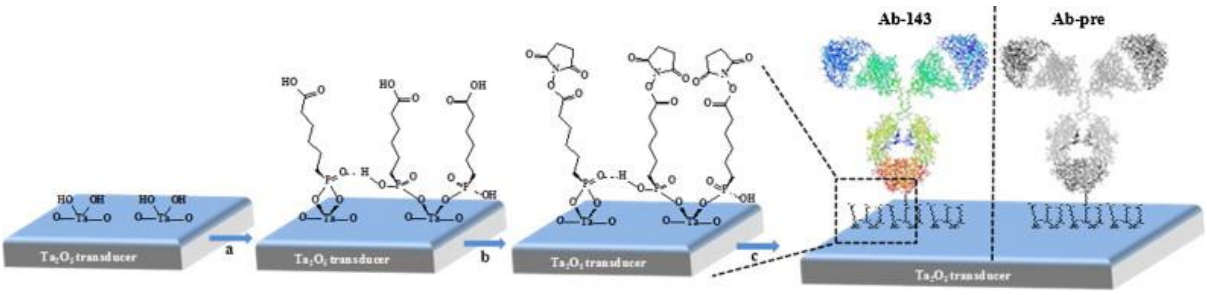

Fig. 7. Covalent immobilization of antibodies onto Ta_2O_5 a carboxylic acid terminated organophosphonate followed by activation of the surface with NHS and EDC and coupling of the antibodies by formation of an amide linkage. [reprinted with permission of ref. [133]].

Modification of silicon and silicon nitride surfaces. Silicon and silicon nitride (Si_3N_4) surfaces can be prepared for modification by first etching to remove any native oxide and then deliberately oxidizing to form a thin continuous oxide layer. As an example, Rong and co-workers used this approach to develop a label free DNA sensor based on porous silicon (PSi). The surface was cleaned, thermally oxidized, and then modified with an amino-terminated silane. The probe oligonucleotides were then covalently attached to the $-NH_2$ surface groups using glutaraldehyde as a crosslinker [135, 136] (Scheme 3d).

Al-Jawdah *et al.* [137] developed a waveguide biosensor for the detection of mycotoxins (in particular, aflatoxin B1) using an aptamer assay. First, the silicon nitride surface was functionalized with an amine terminated silane then a hetero-bifunctional crosslinker (succinimidyl 4-(N-maleimidomethyl)cyclohexane-1-carboxylate, SMCC) was used for the covalent immobilization of the SH-terminated aptamers. In a related example [59, 138], a silicon nitride waveguide was functionalized using a hyperbranched carbosilane polymer for the detection of a chemical warfare agent at trace concentration in the gas phase. The polymer had hexafluoro-isopropanol-terminated groups that selectively interact by hydrogen bonding with gas phase analytes such as nerve agents or nitroaromatics.

Other strategies involve modification of the surface by reacting Si-H bonds, formed by HF etching of the silicon and Si_3N_4, with alkene moieties (hydrosilylation, Scheme 3d) [139]. Qiao *et al*. developed the formation of carboxylic acid–terminated monolayers in porous silicon using this hydrosilylation process. The surface can then be further modified by coupling the carboxylate to any amino-terminated peptide. In this case the group describes the application in a label free protease biosensor [140, 141]. Another approach was introduced by De Stefano *et al.* [142], using photo-activated chemical modification of porous silicon to prepare DNA biosensors. The PSi surface was exposed to UV irradiation in a solution of a carboxylic acid terminated alkene, causing a photochemical hydrosilylation reaction, and producing a carboxylic acid-terminated surface which was subsequently used to couple an amino-terminated DNA strand.

Bañuls and co-workers formed N-H bonds after removal of the native oxide layer on the Si_3N_4. They describe the modification of Si_3N_4 waveguides by direct attachment using glutaraldehyde. This methodology allows the immobilization of amine-terminated biomolecules [143].

Although these chemical modifications of porous Si and Si_3N_4 achieve more stable and reproducible monolayers compared to the silanization methodology, they require anhydrous conditions, the use of HF, and exposure to organic solvents and extended reaction times.

Choice of modification strategy. Ultimately the choice of the biomolecule immobilization strategy depends on the purpose of the study and the characteristics of the analyte and sample. Critical factors

in biosensor functionalization include the selectivity and anti-fouling properties of the biorecognition layer. Consequently, there is extensive interest in developing and optimizing label-free biosensors that ensure detection selectivity whilst, at the same time, minimizing non-specific adsorption. Some strategies have been developed to reduce non-specific adsorption from clinical samples. These surfaces are characterized by their biocompatible, hydrophilic, and anti-fouling properties.

The immobilization of polyethylene glycol (PEG) derivatives has been extensively investigated in the use of SAMs for biomedical applications [128, 144, 145] (Scheme 3c). Waveguides have been modified with poly (L-Lysine)-g-poly (ethylene glycol) (PLL), a polymer that spontaneously adsorbs onto metal oxide surfaces from aqueous solution providing a fast and convenient way to modify the biosensor surface [146-149]. Alternative approaches are based on the use of saccharides, such as dextran, gelatin and heparin [150, 151]. For example, Adrian *et al*. reported an immunosensor based on dextran biofunctionalization for the detection of sulfonamide antibiotic residues in milk. They functionalized the waveguide with a photopolymer layer that allowed the covalent immobilization of biomolecules after exposure to UV light [152].

Blocking layers are often used to overcome non-specific adsorption in biosensors and a number of strategies have been employed, for instance proteins (BSA, casein, ovalbumin), surfactant (Tween), or blocking buffers. Nevertheless, the problem has not been completely solved and it is still a challenge to minimize the effects of non-specific adsorption in label-free analyses.

It is clear from the above that a wide range of chemistries, commercial reagents and biorecognition elements suitable for application to WERS-based biosensors already exist and can be directly applied once a suitable initial chemical surface modification of the waveguide has been made.

Chemical treatment and modification of the waveguide film will undoubtedly impact the waveguiding characteristics but this effect can be minimized through material choice and the selected treatment process. The selection of materials such as Ta_2O_5 and Si_3N_4 which are resistant to corrosion and are not damaged by physical treatments means that a waveguide can be chemically modified with minimal effect on the surface roughness, thus limiting scattering losses at the waveguide-core/superstrate interface and maximizing the interaction of the pump with the target analytes. Self-assembled monolayers of organosilane, organophosphonate or alkene derivatives introduce a very thin (typically 1-3 nm), ordered layer with a refractive index of approximately 1.5, which can be assumed to have a negligible effect on the overall WERS signal. Therefore, a biocompatible sensor with a good signal-to-noise ratio can be realized by careful selection of the materials and the functionalization method.

Review of Recent WERS Implementations

Rising demand for point-of-care devices for clinical diagnostics, the success of SERS as a diagnostic approach and the enormous advances in integrated silicon photonics and optoelectronic instrumentation since 2000 has reignited interest in WERS. There have recently been numerous WERS implementations that demonstrate the capability of the technique in realizing efficient Raman excitation and collection at waveguide surfaces. In this section, we review some of the recent work on WERS, highlighting how the various implementations differ from one another and appraising the methods and practices used in such implementations.

In [76], Dhakal *et al.* utilized a high contrast single mode Si_3N_4 strip waveguide (cross-section of 700 nm × 220 nm on top of a 2.4 μm silica cladding on a silicon substrate) to excite, collect and enhance the Raman signal using the evanescent field of the guided mode. Furthermore, several waveguide lengths of up to 8.1 cm were used and were wound up to form spirals. The waveguide was used to sense isopropyl alcohol (IPA), which was applied such that it covered the entire upper cladding of the

waveguide. An intense Raman peak at 819 cm^{-1} (839 nm) due to the in-phase C-C-O stretch vibration was observed, the conversion efficiency ($\rho\sigma\eta_o$) of which was measured to be 10^{-11} cm^{-1}. In addition, the authors demonstrated a good agreement between their experimental results and theoretical predictions (which were based on the same equations summarized in the "Theoretical Framework for WERS" section of this review). A point of note about this demonstration is that the moderate waveguide transmission loss (2.4 dB/cm) prevents seeing any further advantage from using longer waveguide lengths, as demonstrated by the authors' experimental and theoretical plots of $\xi(L)$ as a function of waveguide length, reproduced here in Fig. 8. This renders the implementation of spirals unnecessary except for ultra-compact photonic devices unless propagation losses are significantly improved in the future.

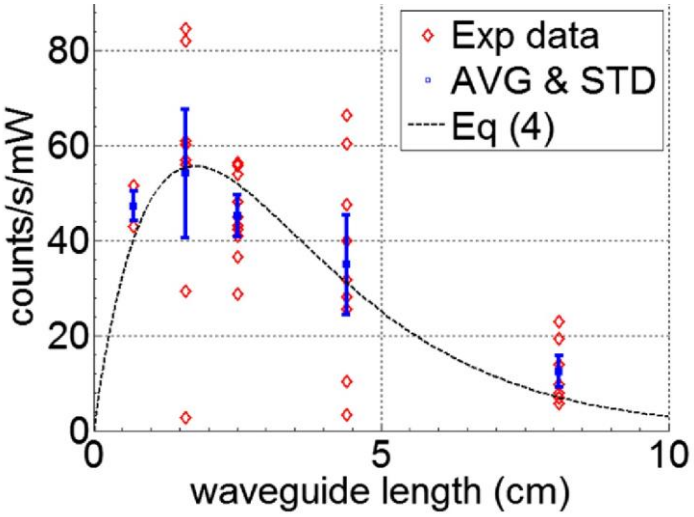

Fig. 8 $\xi(L)$ for 819 cm^{-1} peak due to IPA measured using waveguides of several lengths. Red diamond markers: actual measured data. Blue solid square with error bars: mean and standard deviation. Black dashed line: theoretical fit, to respective equations as a guide for the eye [76]. Reprinted with permission from [76] The Optical Society.

In [87], Dhakal *et al.* extended their work by conducting a systematic experimental and theoretical study on the effect of the waveguide geometry and fundamental-mode polarization on the specific conversion efficiency η_o. The study contrasted two waveguide designs, strip and slot, and again used IPA as an analyte. Si_3N_4 strip waveguides of widths w = 550 nm and w = 700 nm, and Si_3N_4 slot waveguides with slot width s = 150 nm and total waveguide width w = 700 and w = 800 were studied. Using the definitions of TE and TM polarization in Fig. 4, Figure 9 shows that for the 700 nm wide strip waveguides, the average efficiency η_o for the TM polarization was approximately 2.5 times larger than for TE polarization, while for the 700 nm wide slot waveguides (s = 150 nm) excited with TE polarized light, about 5 fold enhancement of the estimated η_o was obtained compared to strip waveguides of the same width. For strip waveguides the TM polarization generally performs better than TE polarized modes due to the fact that the discontinuity of the electric field at the core-cladding interface of the TM modes leads to higher field at the analyte location. However, slot waveguides exhibited similar performance in both polarizations due to the reduced field enhancement in the TM polarization as shown in Figure 4 c & f. Despite the performance advantage of slot waveguides in TM polarization, in terms of efficiency and low background, there remain the non-trivial challenges of loss due to slot waveguide side-wall roughness and pump input launching. Nevertheless, such waveguides may be attractive to use in Raman applications where the background emission provides the limiting noise source.

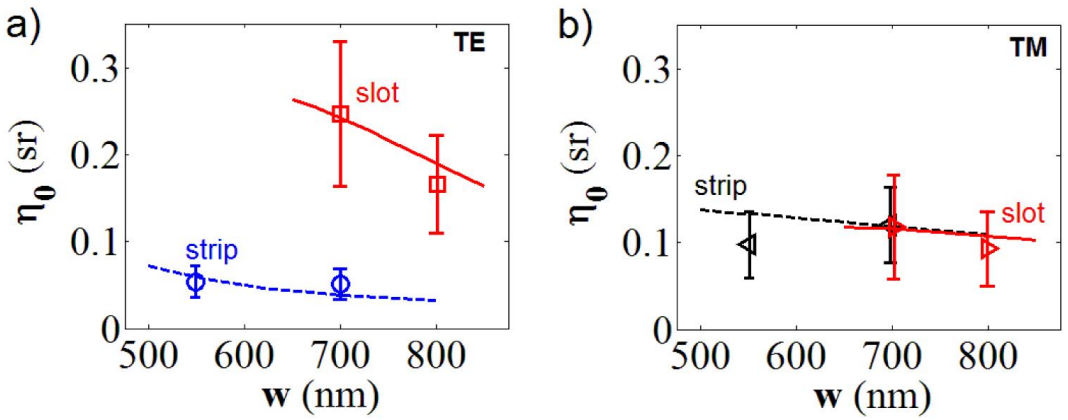

Fig. 9. The theoretical and experimental values of η_0 obtained for a) TE modes and b) TM modes of Si_3N_4 waveguides. The markers represent the estimated experimental values obtained from the LSE fit of the experimental data. The error bars represent the measurement and estimation errors. Lines represent the theoretical curves. The red solid lines are the theoretical curve for slot waveguides with s = 150 nm. The blue and black dashed lines are the theoretical curves for TE and TM polarizations respectively for strip waveguides. Circle: TE polarization, strip waveguides. Left handed triangles: TM polarization, strip waveguides. Right handed triangles: TM polarization, slot waveguides. Square: TE polarization, slot waveguides [87]. Reprinted with permission from [87] The Optical Society.

In [58], Dhakal *et al.* reported waveguide enhanced Raman detection of a monolayer and real-time measurements of the hybridization of DNA strands and the density of submonolayers of biotin−streptavidin complex located on top of the waveguide. A monolayer of rhodamine molecules on an aminosilanized Si_3N_4 slot waveguide was used and the results were compared to those from a commercial Raman microscope (Fig. 10). Figure 10 shows than even when ignoring the high coupling losses into the waveguide (which were 18 dB in this case), a much stronger Raman signal is observed from the WERS device due to the strong waveguide enhancement of the Raman signal. By correcting for the waveguide coupling losses and comparing the signal-to-noise ratio (SNR) of the WERS device and the commercial microscope as a function of the density of the molecules or the cross-section of the molecules, more than two orders of magnitude improvement in the SNR is expected from the waveguide in comparison to the Raman microscope. This could be further increased by reducing the shot noise of the waveguide background emission by material engineering or waveguide design.

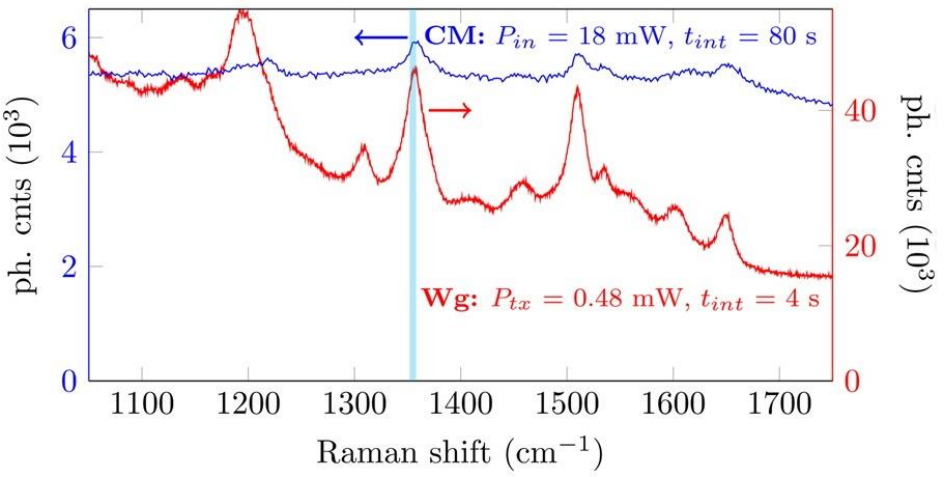

Fig. 10 The measured spectra of a Rhodamine monolayer obtained from a commercial Raman microscope (CM, P_{in} = 18 mW and t_{int} = 80 s, in blue with left blue axis), in contrast to the spectra obtained from the 1 cm slot waveguides (Wg, P_{in} = 30 mW, P_{tx} = 0.48 mW, and t_{int} = 4 s, in red with right red axis). [Reprinted (adapted) with permission from [58]. Copyright (2021) American Chemical Society].

C. C. Evans *et al.* reported in the utilization of a TiO_2-based waveguide to demonstrate high Raman conversion efficiencies [79]. The shorter wavelength of 532 nm was used to exploit the low auto-fluorescence of their material, benefitting from the higher Raman cross-section at shorter wavelengths. This, along with the high refractive index of TiO_2 contributed towards the high conversion efficiencies achieved. The conversion efficiency for the TiO_2 based WERS device (pumped at 532 nm) was compared with that achieved by the Si_3N_4 WERS device (pumped at 785 nm) in [76] when using IPA as an analyte. Comparing the power conversion efficiency (Raman output to launched pump) for the two material platforms yielded an experimental efficiency more than 50 times larger than previous experimental values in silicon nitride. Part of this was due to comparing TM polarized operation with TE polarized operation, a factor of about 5 was due to the shorter pump wavelength, with the remainder being due to the high refractive index of TiO_2. Despite these advantages, the high TiO_2 waveguide losses currently hinder the platform from realizing its full potential and the wavelength limits its use to analyzing materials with negligible auto-fluorescence.

S. A. Holmstrom *et al.* reported in [59] the first demonstration of Raman scattering measurements of trace gases using a rib Si_3N_4 waveguide pumped at 1064 nm. Raman spectra of ethyl acetate, methyl salicylate, and dimethyl sulfoxide were successfully detected at concentrations of 600 ppm, 360 ppb, and 7.6 ppb, respectively. Furthermore, the authors calculated that Raman signal enhancement of 4.2×10^9 cm^{-1} was achieved using the WERS sensor to detect dimethyl sulfoxide (DMSO) compared to free-space micro-Raman scattering of the trace gas. The most significant contribution to the enhancement, in this case, comes from the thin, transparent, hypersorbent polymer cladding layer that acts to partition and concentrates the analyte of interest, increasing the density of the analyte molecules by a factor of 10^8 compared to the ambient environment. Figure 11 shows the Raman spectra collected from the Si_3N_4 waveguide prior to and during exposure to dimethyl sulfoxide. This WERS demonstration shows the potential of realizing hand-held devices capable of detecting trace concentrations of gas-phase chemicals, a feat that has so far eluded conventional and hollow-core fiber-based Raman spectroscopy systems. Furthermore, the authors envision the possibility of large-scale fabrication of waveguide arrays with different coatings to sorb and detect different classes of vapors or gases.

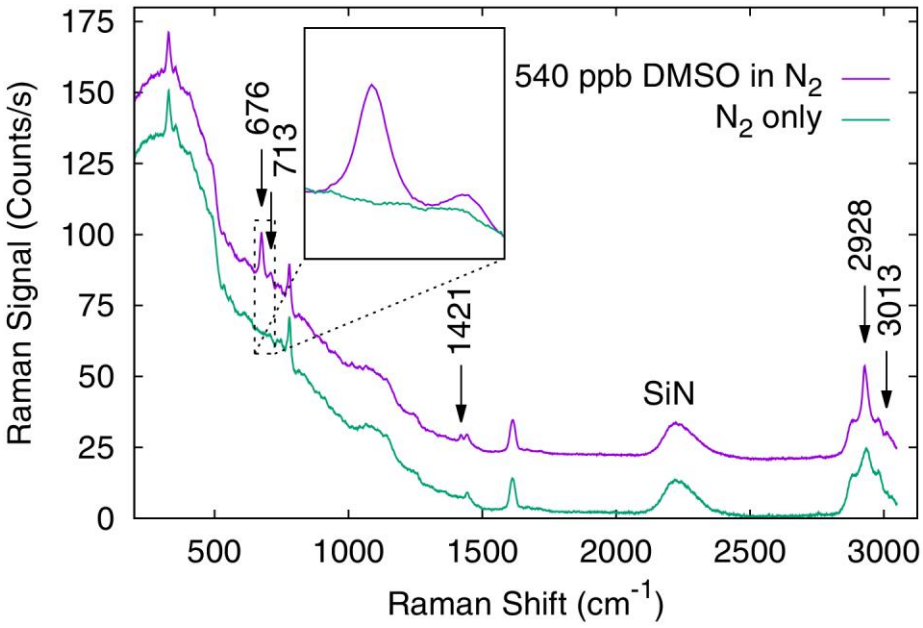

Fig. 11 Raman spectra collected from the Si_3N_4 waveguide prior to and during exposure to dimethyl sulfoxide. Reprinted with permission from [59] The Optical Society.

In [153], Z. Wang *et al.* conducted an experimental and theoretical study that compares the collection of a Raman signal from the waveguide end with that from the waveguide surface. A 110 nm film high tantalum pentoxide waveguide was used as the sensing element (pumped at 637 nm), while toluene was used as the model analyte. A 40-fold greater signal was collected from the waveguide end compared to the waveguide surface, which was also verified with the simulations of angular and spatial Raman emission distributions. Such an enhancement stems from the efficient collection of power from dipoles near the surface into the waveguide film and substrate, combined with the long interaction length.

A demonstration of waveguide enhanced stimulated Raman scattering (SRS) was reported by H. Zhao *et al.* in [62]. In addition to the conventional waveguide enhancement, SRS provides a further enhancement by stimulating the specific molecular transitions through the use of a second laser beam, whose frequency is selected such that the frequency difference between the two beams matches the vibrational frequency of the molecule. The implementation in [62] used a strip Si_3N_4 waveguide whose design took into account the trade-off between achieving acceptable propagation loss and a strong overlap between the evanescent field and the analyte. The Raman response of dimethyl sulfoxide was measured, and a signal enhancement approaching five orders of magnitude in comparison to conventional spontaneous Raman enhancement was achieved. This enabled the detection of the Raman fingerprints of 280 mM (2%) of DMSO dissolved in water using low-power excitation and a 1 cm long waveguide. While the experimental implementation of the SRS scheme is more complex than the spontaneous Raman schemes, this demonstration provides significant enhancement, and a further performance increase could be realized by addressing the non-optimized aspects of the implementation such as the pump modulation, coupling efficiency and waveguide design.

D. Kita *et al.* have recently demonstrated the first packaged fiber-coupled WERS sensor, integrated with a flow cell to allow sequences of chemical compounds to be applied to the sensing chip [154]. Prior WERS demonstrations had always relied on the use of either free-space lenses or prisms to couple light in and out of the chip. Kita *et al.* addressed the issue of the strong Raman background and fluorescence generated by the coupling input and output fibers by using a 2×2 directional coupler that splits light into two spiral waveguide channels and subsequently collecting the backward-propagating Raman scattered signal at the opposite side of the chip through a collection fiber. In this implementation, the authors used a slot waveguide consisting of two 350 nm strips and a 100 nm slot gap. To enable the conversion from the TE strip mode from the 2×2 coupler to the TE slot mode, a multi-mode interferometer was implemented. The slot waveguides form spirals with 100 µm radius bends, and a waveguide sensing region of 8 cm long. The packaged sensing chip was used to measure the Raman spectra for varying concentrations of IPA in water, from 5% to 100%. The authors experimentally compared the signal-to-background ratio performance of the back-scattered collection to the forward-scattered collection and found that the latter scheme exhibits a significantly worse background noise performance due to the substantial Raman and fluorescence signal generated in the fiber, and calculated that the pump rejection ratio afforded by the back-scattered collection is approximately -9.6 dB. The authors also confirm that while slot waveguides provide high specific conversion efficiency, their high scattering losses due to the additional sidewall roughness may make them inferior to the simpler TM strip waveguides, whose lower losses compensate for their lower specific conversion efficiency.

Waveguide-enhanced Raman devices can benefit from on-chip integration of photonic components. These potentially remove the need for some off-chip components such as filters and couplers or at least relaxes their specification and, perhaps more significantly, allows for on-chip separation of

Raman signal from SNR-limiting background, particularly in backscattering WERS configurations. Such components may be defined lithographically with the WERS waveguides without adding process steps, and therefore at no additional cost assuming that better lithographic resolution is not required. There have been several demonstrations of on-chip component integration for applications to WERS. Nie et al. [155] demonstrated a high extinction ratio (68.5dB) pump rejection filter using cascaded grating-assisted contra-directional couplers on a Si_3N_4 platform, with transmission of about -5.6dB outside the reflection band, suitable for pump-rejection in WERS. A key attribute was the coupling of the rejected pump into a separate waveguide to the pump input, avoiding back-reflection into the pump laser. Kita et al. [154] used an integrated on-chip directional coupler in a backscattered a Si_3N_4 WERS configuration to separate the backward-travelling Raman signal from the predominantly forward-travelling pump and the Raman/fluorescence background (predominantly generated in the input fibre carrying the pump) and potentially improve the SNR by a factor of up to 20dB depending on the source of the background. Reynkens et al. [156] also demonstrated background suppression in a backscattered Si_3N_4 plasmonic WERS configuration, in this case using a multimode interferometer (MMI) rather than a directional coupler. Background emission from the Si_3N_4 waveguides was considered the fundamental limitation to SNR and the MMI is expected to contribute a lower background due to its shorter length. Tyndall et al. [157] integrated directional coupler lattice filters for Si_3N_4 WERS in a forward- and back-scattering configuration, showing significant reduction in collected input fibre background and collected pump, the latter important for reducing output fibre background.

Conclusions and Future Prospects

Biosensors based on waveguide-enhanced Raman spectroscopy have the potential to exhibit the advantages of SERS and SERRS approaches in terms of specificity and sensitivity, combined with the use of robust, low-loss materials, reliable lithographic fabrication techniques, and the opportunity for on-chip integration with compact instrumentation. In addition, WERS has the practical advantage of an optical path for excitation and collection which does not pass through the sample, offering opportunities for simple sample handling and presentation, and access to both polarizations for more complete study of the Raman polarizability tensor of bound molecules. WERS achieves comparable Raman enhancement to SERS by building up the signal with waveguide length, meaning that it is not suitable for single-molecule detection (without addition of plasmonic nanostructures) and that low waveguide losses must be achieved for good performance.

While WERS was originally demonstrated in the 1970s, research activity has become reinvigorated recently, due to the need for cheap, compact, reliable, ideally label-free, point-of-use devices and building on the electromagnetic insights and advances in chemistry harnessed by SERS, but frustrated by poor repeatability. Recent research has optimized waveguide designs, addressed fabrication challenges, investigated new material platforms and implemented packaged sensors, which have together resulted in improving the Raman conversion efficiencies and sensitivity of detection of WERS and led to impressive demonstrations such as monolayer [58] and trace gas detection [59].

The most promising candidate materials to emerge for WERS waveguides are high-index dielectrics such as Si_3N_4, TiO_2 and Ta_2O_5, all of which perform well, and the challenge is now (i) to minimize the waveguide losses to exploit the growth of Raman signal with length, (ii) to minimize the fluorescent/Raman background from the waveguide materials, to reduce shot noise which has emerged as a fundamental limit to WERS performance and (iii) to realize surface modification approaches appropriate to attach receptors on dielectric films. The majority of recent WERS demonstrations have focused on using strip or slot waveguides to generate the strong electric fields

required to sense the chemical analyte, and detailed work has been conducted to understand the influence of waveguide structural parameters and modal properties on the Raman figure of merit [58, 78]. Slot waveguides show higher Raman conversion efficiencies than strip waveguides, in principle, but the larger interaction of modal fields with the roughness of etched surfaces in the slot waveguide can cause increased loss, which may limit efficiency. Waveguides designed to be sensitive to surface films tend also to be sensitive to surface roughness. However, the limit of detection is determined by noise power as well as signal power, and slot waveguides generate lower background from the waveguide materials (and hence lower shot noise) as the modal power fraction in the core is lower.

Before the attachment of the receptors on the dielectric films, the surface needs to be chemically modified to introduce the functional groups that allow for the immobilization of the biomolecule. Predominantly for WERS substrates, the chemical modification strategies can be classified into two main groups, chemical modification of metal oxide surfaces and chemical modification of silicon and silicon nitride surfaces where we have oxide-free, H-terminated surfaces after etching the native oxide. Silanization has been widely employed for surface modification because it is relatively easy to carry out and the silane reagents are readily available. However, this technique presents some disadvantages as the reproducible deposition and formation of well-defined monolayers is exceedingly difficult. The major problems lie in the polymerization and the hydrolysis of Si-O-Si causing issues in homogeneity and stability. Although silanization is the most extensively used approach in the literature, this is an area where there is scope for improvement. The use of phosphonates for attachment to metal oxide surfaces generally provides more stable and better-ordered monolayers [131]. Organophosphonate derived SAMs are more resistant to hydrolysis under physiological conditions and do not require pre-treatment of the surface with acid to obtain high coverage [124]. Phosphonate SAMs show excellent biocompatibility and chemical resistance under aqueous conditions and in biological samples. As mentioned earlier, the chemical modifications of porous Si and Si_3N_4 achieve more stable and reproducible monolayers compared to the silanization methodology; nonetheless, they require anhydrous conditions, the use of HF, and exposure to organic solvents and extended reaction times.

Another hurdle that limits the performance of WERS systems is the high pump laser input coupling losses. Most WERS demonstrations have either used free-space end-fire coupling using high numerical aperture (NA) aspheric or microscope objective lenses into nanophotonic strip waveguides [58, 59], with an insertion loss of approximately 8 dB [58], or prism coupling using a high-refractive index prism into ultrathin slab waveguides [153], with a minimum insertion loss of order 5 dB. Furthermore, end-fire coupling suffers from requiring end-facet preparation and high-accuracy optical alignment using expensive alignment stages, as well as being sensitive to vibrations, while prism-coupling requires additional micro-optics and fine control of coupling strength. Overcoming these limitations by exploring more complex coupling strategies such as the use of inverse tapers [158] and trident structures [159] can be pursued. An alternative approach is that of D. Kita *et al.* [154] who utilized fibers bonded to the input and output facets, and which resulted in a theoretical coupling efficiency of 3 dB, eliminating the need for alignment controllers and minimized vibration sensitivity, all of which contributed to enhancing the practicality of a packaged sensor for applications requiring field testing.

However, in a point-of-care setting, frequent replacement of disposable WERS chips and thus easy alignment by the operator may be required and in this case slab waveguides combined with grating couplers may be preferred [160]. Slab waveguides are simple to fabricate and have low loss and similar Raman excitation efficiencies as strip waveguides, though they have lower Raman collection efficiencies due to their lack of lateral confinement. They also have a potential advantage in terms of polarization-resolved studies of ordered molecular layers on their plane surfaces. Grating couplers

have matured remarkably in recent years [161], benefiting from both extensive analytical and numerical design studies and significant advances in nanofabrication technology, with insertion loss below 1 dB demonstrated. Grating couplers also exhibit good translational alignment tolerance and indifference to end-facet quality, which offer significant benefits to the practicality of WERS sensors. Furthermore, their most significant limitation, namely their narrow bandwidth, is not problematic for pump input coupling in WERS applications since mode excitation uses light from a narrow linewidth laser. Such gratings can be readily designed to pass the Stokes-shifted Raman emission, allowing for backward collection from the end facet if required.

To select an optimum WERS chip configuration, it is necessary to include not only the effect of waveguide type and geometry on the Raman conversion efficiency but to also account for other parameters such as the surface and side wall roughness, the generation of background emission, and the light coupling efficiencies through the system from laser to spectrometer. With further optimization of waveguide design and input and output coupling methodology, and improved material engineering, waveguide-enhanced Raman sensors have the potential to achieve ultra-high sensitivities that rival the sensitivity of SERS-based instruments, while simultaneously being low cost, avoiding the need for complex and delicate noble metal nanostructures, and offering a high degree of miniaturization, leading to a new generation of highly versatile sensors suitable for a wide array of biological, industrial and environmental sensing applications.

Acknowledgements

This work was funded by the UK Engineering and Physical Sciences Research Council (EPSRC) under Grant EP/R011230/1, “Flexible Raman biosensing platform for low-cost health diagnostics”. M.N.Z. acknowledges financial support from the Royal Academy of Engineering. Z.L. acknowledges financial support from the China Scholarship Council (No. 201808430227) and B.B thanks the Defence Science and Technology Laboratory (contract no. DSTLX-1000128554) for supporting an EPSRC industrial CASE award.

Vocabulary

Optical waveguide, a geometrical structure that confines and guides electromagnetic waves (specifically light) in a particular direction; Evanescent field, an electromagnetic wave that propagates parallel to the core-cladding interface of the waveguide, and whose intensity decays exponentially with distance from the interface; Integrated photonics; a branch of photonics in which multiple optical devices and functions are integrated into a single circuit, fabricated onto the surface of a flat substrate; Biosensor, a sensing device that integrates a biological receptor (e.g. antibody, DNA probe or enzyme) with a detection element (optical, electrochemical or mechanical) producing specific recognition events between the bioreceptor and the analyte of interest through physicochemical changes that can be transformed into a measurable signal; Surface biofunctionalization, a set of well-established methods, based on chemical processes, for attaching biological molecules to functional groups presented on a surface in order to capture the target analyte for the recognition event.

References

1. L. Jason-Moller, M. Murphy, and J. Bruno, *Overview of Biacore Systems and Their Applications.* Current Protocols in Protein Science, 2006. **45**(1).
2. E. Benito-Peña, M.G. Valdés, B. Glahn-Martínez, and M.C. Moreno-Bondi, *Fluorescence based fiber optic and planar waveguide biosensors. A review.* Analytica Chimica Acta, 2016. **943**: p. 17-40.
3. P.B. Yi Xu, Xiaodong Zhou, Yuriy Akimov, Ching Eng Png, Lay-Kee Ang, Wolfgang Knoll and Lin Wu, Optical Refractive Index Sensors with Plasmonic and Photonic Structures: Promising and Inconvenient Truth, Adv. Optical Mater. 2019, 1801433.
4. G. Bartman and M. Fletcher, *UV Fluorescence for Monioring Oil and Grease in Produced Water- Real Data from the Field*, in *12th Annual Produced Water Seminar*. 2002: Houston, TX.
5. X. Fan and I.M. White, *Optofluidic microsystems for chemical and biological analysis.* Nature Photonics, 2011. **5**(10): p. 591-597.
6. U. Frank, *A review of fluorescence spectroscopic methods for oil spill source identification.* Toxicological & Environmental Chemistry Reviews, 1978. **2**(3): p. 163-185.
7. J. Jehlička, H.G.M. Edwards, and A. Culka, *Using portable Raman spectrometers for the identification of organic compounds at low temperatures and high altitudes: exobiological applications.* Philosophical Transactions of the Royal Society A: Mathematical, Physical and Engineering Sciences, 2010. **368**(1922): p. 3109-3125.
8. P. Rohde, J.A. Busch, R.H. Henkel, D. Voss, and O. Zielinski, *Detection and identification of hydrocarbons in marine waters using time-resolved laser-fluorescence: Set-up and first results of a new submersible sensor*, in *OCEANS 2009-EUROPE*. 2009, IEEE.
9. E. Stern, J.F. Klemic, D.A. Routenberg, P.N. Wyrembak, D.B. Turner-Evans, A.D. Hamilton, D.A. LaVan, T.M. Fahmy, and M.A. Reed, *Label-free immunodetection with CMOS-compatible semiconducting nanowires.* Nature, 2007. **445**(7127): p. 519-522.
10. L. Zhang, G. Tian, J. Li, and B. Yu, *Applications of Absorption Spectroscopy Using Quantum Cascade Lasers.* Applied Spectroscopy, 2014. **68**(10): p. 1095-1107.
11. S.K. Chang, I. Pavlova, N. Marin, M. Follen, and R. Richards-Kortum, *Fluorescence spectroscopy as a diagnostic tool for detecting cervical pre-cancer.* Gynecologic Oncology, 2005. **99**(3): p. S61-S63.
12. A. Ide-Ektessabi and M. Rabionet, *The Role of Trace Metallic Elements in Neurodegenerative Disorders: Quantitative Analysis Using XRF and XANES Spectroscopy.* Analytical Sciences, 2005. **21**(7): p. 885-892.
13. L. Bachmann, D.M. Zezell, A.d.C. Ribeiro, L. Gomes, and A.S. Ito, *Fluorescence Spectroscopy of Biological Tissues—A Review.* Applied Spectroscopy Reviews, 2006. **41**(6): p. 575-590.
14. J. Sádecká and J. Tóthová, *Fluorescence spectroscopy and chemometrics in the food classification − a review.* Czech Journal of Food Sciences, 2008. **25**(No. 4): p. 159-174.
15. F. Zaera, *New advances in the use of infrared absorption spectroscopy for the characterization of heterogeneous catalytic reactions.* Chem. Soc. Rev., 2014. **43**(22): p. 7624-7663.
16. K.-i. Miyamoto, P. Yamada, R.-t. Yamaguchi, T. Muto, A. Hirano, Y. Kimura, M. Niwano, and H. Isoda, *In situ observation of a cell adhesion and metabolism using surface infrared spectroscopy.* Cytotechnology, 2007. **55**(2-3): p. 143-149.
17. M.S. Shumate, R.T. Menzies, W.B. Grant, and D.S. McDougal, *Laser absorption spectrometer: remote measurement of tropospheric ozone.* Applied Optics, 1981. **20**(4): p. 545.
18. S.P. Singhal, *Atomic Absorption Spectroscopy in Forensic Chemistry.* Canadian Society of Forensic Science Journal, 1974. **7**(1): p. 7-17.
19. H. Edner, P. Ragnarson, S. Spännare, and S. Svanberg, *Differential optical absorption spectroscopy (DOAS) system for urban atmospheric pollution monitoring.* Applied Optics, 1993. **32**(3): p. 327.

20. T. Schädle and B. Mizaikoff, *Mid-Infrared Waveguides: A Perspective.* Applied Spectroscopy, 2016. **70**(10): p. 1625-1638.
21. G.S. Bumbrah and R.M. Sharma, *Raman spectroscopy – Basic principle, instrumentation and selected applications for the characterization of drugs of abuse.* Egyptian Journal of Forensic Sciences, 2016. **6**(3): p. 209-215.
22. G. Turrell and J. Corset, *Raman Microscopy: Developments and Applications*. 1996: Elsevier Science.
23. R.F. Begley, A.B. Harvey, and R.L. Byer, *Coherent anti-Stokes Raman spectroscopy.* Applied Physics Letters, 1974. **25**(7): p. 387-390.
24. M. Fan, G.F.S. Andrade, and A.G. Brolo, *A review on the fabrication of substrates for surface enhanced Raman spectroscopy and their applications in analytical chemistry.* Analytica Chimica Acta, 2011. **693**(1-2): p. 7-25.
25. K. Kneipp, M. Moskovits, and H. Kneipp, *Surface-Enhanced Raman Scattering: Physics and Applications*. 2006: Springer Berlin Heidelberg.
26. E.C. Le Ru and P.G. Etchegoin, *Raman spectroscopy and related optical techniques*, in *Principles of Surface-Enhanced Raman Spectroscopy*. 2009, Elsevier. p. 29-120.
27. S. Schlücker, *Surface-Enhanced Raman Spectroscopy: Concepts and Chemical Applications.* Angewandte Chemie International Edition, 2014. **53**(19): p. 4756-4795.
28. D. Cialla, T. Deckert-Gaudig, C. Budich, M. Laue, R. Möller, D. Naumann, V. Deckert, and J. Popp, *Raman to the limit: tip-enhanced Raman spectroscopic investigations of a single tobacco mosaic virus.* Journal of Raman Spectroscopy, 2008. **40**(3): p. 240-243.
29. S. Dochow, C. Beleites, T. Henkel, G. Mayer, J. Albert, J. Clement, C. Krafft, and J. Popp, *Quartz microfluidic chip for tumour cell identification by Raman spectroscopy in combination with optical traps.* Analytical and Bioanalytical Chemistry, 2013. **405**(8): p. 2743-2746.
30. W.L. Peticolas, *Raman spectroscopy of DNA and proteins*, in *Methods in Enzymology*. 1995, Elsevier. p. 389-416.
31. K. Kneipp, Y. Wang, H. Kneipp, L.T. Perelman, I. Itzkan, R.R. Dasari, and M.S. Feld, *Single Molecule Detection Using Surface-Enhanced Raman Scattering (SERS).* Physical Review Letters, 1997. **78**(9): p. 1667-1670.
32. E.C. Le Ru and P.G. Etchegoin, *Single-Molecule Surface-Enhanced Raman Spectroscopy.* Annual Review of Physical Chemistry, 2012. **63**(1): p. 65-87.
33. D. Zhang, Y.-C. Wu, M. Yang, X. Liu, C.Ó. Coileáin, M. Abid, M. Abid, J.-J. Wang, I. Shvets, H. Xu, B.S. Chun, H. Liu, and H.-C. Wu, *Surface enhanced Raman scattering of monolayer MX2 with metallic nano particles.* Scientific Reports, 2016. **6**(1).
34. M. Fan, G.F.S. Andrade, and A.G. Brolo, *A review on recent advances in the applications of surface-enhanced Raman scattering in analytical chemistry.* Analytica Chimica Acta, 2020. **1097**: p. 1-29.
35. J. Langer, D. Jimenez de Aberasturi, J. Aizpurua, R.A. Alvarez-Puebla, B. Auguié, J.J. Baumberg, G.C. Bazan, S.E.J. Bell, A. Boisen, A.G. Brolo, J. Choo, D. Cialla-May, V. Deckert, L. Fabris, K. Faulds, F.J. García de Abajo, R. Goodacre, D. Graham, A.J. Haes, C.L. Haynes, C. Huck, T. Itoh, M. Käll, J. Kneipp, N.A. Kotov, H. Kuang, E.C. Le Ru, H.K. Lee, J.-F. Li, X.Y. Ling, S.A. Maier, T. Mayerhöfer, M. Moskovits, K. Murakoshi, J.-M. Nam, S. Nie, Y. Ozaki, I. Pastoriza-Santos, J. Perez-Juste, J. Popp, A. Pucci, S. Reich, B. Ren, G.C. Schatz, T. Shegai, S. Schlücker, L.-L. Tay, K.G. Thomas, Z.-Q. Tian, R.P. Van Duyne, T. Vo-Dinh, Y. Wang, K.A. Willets, C. Xu, H. Xu, Y. Xu, Y.S. Yamamoto, B. Zhao, and L.M. Liz-Marzán, *Present and Future of Surface-Enhanced Raman Scattering.* ACS Nano, 2019. **14**(1): p. 28-117.
36. W.E. Smith, *Practical understanding and use of surface enhanced Raman scattering/surface enhanced resonance Raman scattering in chemical and biological analysis.* Chemical Society Reviews, 2008. **37**(5): p. 955.
37. A. Otto, *The "chemical" (electronic) contribution to surface-enhanced Raman spectroscopy.* J. Raman Spectrosc., 2005. **36**: p. 497-509.

38. A. Campion and P. Kambhampati, *Surface-enhanced Raman scattering.* Chem. Soc. Rev., 1998. **27**: p. 241-250.
39. M. Moskovits, *Surface-enhanced Raman spectroscopy: a brief retrospective.* J. Raman Spec., 2005. **36**: p. 485-496.
40. A. Otto, I. Mrozek, H. Grabhorn, and W. Akemann, *Surface-enhanced Raman scattering.* J. Phys. Condens. Matter, 1992. **4**: p. 1143-1212.
41. Z.-Q. Tian, B. Ren, and D.-Y. Wu, *Surface-enhanced Raman scattering: from noble to transition metals and from rough surfaces to ordered structures.* J. Phys. Chem. B, 2002. **106**: p. 9463-9483.
42. M. Moskovits, *Surface selection rules.* J. Chem. Phys., 1982. **77**: p. 4408-4416.
43. J.S. Suh and M. Moskovits, *Surface-enhanced Raman spectroscopy of amino acids and nucleotide bases adsorbed on silver.* J. Am. Chem. Soc., 1986. **108**(16): p. 4711-4718.
44. M. Moskovits and J.S. Suh, *Surface selection rules for surface-enhanced Raman spectroscopy: calculations and application to the surface-enhanced Raman spectrum of phthalazine on silver.* J. Phys. Chem., 1984. **88**: p. 5526-5530.
45. X. Gao, J.P. Davies, and M.J. Weaver, *A test of surface selection rules for surface-enhanced Raman scattering: the orientation of adsorbed benzene and monosubstituted benzenes on gold.* J. Phys. Chem., 1990. **94**: p. 6858-6864.
46. I. Bruzas, W. Lum, Z. Gorunmez, and L. Sagle, *Advances in surface-enhanced Raman spectroscopy (SERS) substrates for lipid and protein characterization: sensing and beyond.* The Analyst, 2018. **143**(17): p. 3990-4008.
47. E. Garcia-Rico, R.A. Alvarez-Puebla, and L. Guerrini, *Direct surface-enhanced Raman scattering (SERS) spectroscopy of nucleic acids: from fundamental studies to real-life applications.* Chemical Society Reviews, 2018. **47**(13): p. 4909-4923.
48. S. Laing, K. Gracie, and K. Faulds, *Multiplex in vitro detection using SERS.* Chemical Society Reviews, 2016. **45**(7): p. 1901-1918.
49. G. Sabatte, R. Keir, M. Lawlor, M. Black, D. Graham, and W.E. Smith, *Comparison of surface-enhanced resonance Raman scattering and fluorescence for detection of a labeled antibody.* Anal. Chem., 2008. **80**(7): p. 2351-2356.
50. K. Faulds, R.P. Barbagallo, J.T. Keer, W.E. Smith, and D. Graham, *SERRS as a more sensitive technique for the detection of labelled oligonucleotides compared to fluorescence.* Analyst, 2004. **129**: p. 567-568.
51. M. Jermyn, J. Desroches, K. Aubertin, K. St-Arnaud, W.-J. Madore, E. De Montigny, M.-C. Guiot, D. Trudel, B.C. Wilson, K. Petrecca, and F. Leblond, *A review of Raman spectroscopy advances with an emphasis on clinical translation challenges in oncology.* Physics in Medicine and Biology, 2016. **61**(23): p. R370-R400.
52. A.H. Atabaki, S. Moazeni, F. Pavanello, H. Gevorgyan, J. Notaros, L. Alloatti, M.T. Wade, C. Sun, S.A. Kruger, H. Meng, K. Al Qubaisi, I. Wang, B. Zhang, A. Khilo, C.V. Baiocco, M.A. Popović, V.M. Stojanović, and R.J. Ram, *Integrating photonics with silicon nanoelectronics for the next generation of systems on a chip.* Nature, 2018. **556**(7701): p. 349-354.
53. C. Cornet, Y. Léger, and C. Robert, *Group IV Silicon Lasers*, in *Integrated Lasers on Silicon*. 2016, Elsevier. p. 31-46.
54. Z. Hu, A. Glidle, C.N. Ironside, M. Sorel, M.J. Strain, J. Cooper, and H. Yin, *Integrated microspectrometer for fluorescence based analysis in a microfluidic format.* Lab on a Chip, 2012. **12**(16): p. 2850.
55. D. Huang, P. Pintus, and J.E. Bowers, *Towards heterogeneous integration of optical isolators and circulators with lasers on silicon [Invited].* Optical Materials Express, 2018. **8**(9): p. 2471.
56. T. Mappes, T. Wienhold, U. Bog, C. Vannahme, M.B. Christiansen, A. Kristensen, X. Liu, S. Klinkhammer, U. Lemmer, T. Grossmann, T. Beck, and H. Kalt, *On-chip integrated lasers for biophotonic applications*, in *2012 International Symposium on Optomechatronic Technologies (ISOT 2012)*. 2012, IEEE.

57. S. Clemmen, A. Raza, A. Dhakal, F. Peyskens, A. Subramanian, P. Van Dorpe, P. Wuytens, H. Zhao, E. Ryckeboer, S. Severi, N. Le Thomas, and R. Baets, *Spectroscopic sensing with silicon nitride photonic integrated circuits*, in *Integrated Optics: Devices, Materials, and Technologies XXI*. 2017, SPIE.
58. A. Dhakal, P.C. Wuytens, F. Peyskens, K. Jans, N. Le Thomas, and R. Baets, *Nanophotonic Waveguide Enhanced Raman Spectroscopy of Biological Submonolayers.* ACS Photonics, 2016. **3**(11): p. 2141-2149.
59. S.A. Holmstrom, T.H. Stievater, D.A. Kozak, M.W. Pruessner, N. Tyndall, W.S. Rabinovich, R. Andrew McGill, and J.B. Khurgin, *Trace gas Raman spectroscopy using functionalized waveguides.* Optica, 2016. **3**(8): p. 891.
60. J.S. Kanger, C. Otto, M. Slotboom, and J. Greve, *Waveguide Raman Spectroscopy of Thin Polymer Layers and Monolayers of Biomolecules Using High Refractive Index Waveguides.* The Journal of Physical Chemistry, 1996. **100**(8): p. 3288-3292.
61. J.F. Rabolt, R. Santo, and J.D. Swalen, *Raman Measurements on Thin Polymer Films and Organic Monolayers.* Applied Spectroscopy, 1980. **34**(5): p. 517-521.
62. H. Zhao, S. Clemmen, A. Raza, and R. Baets, *Stimulated Raman spectroscopy of analytes evanescently probed by a silicon nitride photonic integrated waveguide.* Optics Letters, 2018. **43**(6): p. 1403.
63. K.-Q. Lin, J. Yi, S. Hu, B.-J. Liu, J.-Y. Liu, X. Wang, and B. Ren, *Size Effect on SERS of Gold Nanorods Demonstrated via Single Nanoparticle Spectroscopy.* The Journal of Physical Chemistry C, 2016. **120**(37): p. 20806-20813.
64. A. Matikainen, T. Nuutinen, T. Itkonen, S. Heinilehto, J. Puustinen, J. Hiltunen, J. Lappalainen, P. Karioja, and P. Vahimaa, *Atmospheric oxidation and carbon contamination of silver and its effect on surface-enhanced Raman spectroscopy (SERS).* Scientific Reports, 2016. **6**(1).
65. W. Xi, B.K. Shrestha, and A.J. Haes, *Promoting Intra- and Intermolecular Interactions in Surface-Enhanced Raman Scattering.* Analytical Chemistry, 2017. **90**(1): p. 128-143.
66. C. Zong, M. Xu, L.-J. Xu, T. Wei, X. Ma, X.-S. Zheng, R. Hu, and B. Ren, *Surface-Enhanced Raman Spectroscopy for Bioanalysis: Reliability and Challenges.* Chemical Reviews, 2018. **118**(10): p. 4946-4980.
67. K. Okamoto, *Planar optical waveguides*, in *Fundamentals of Optical Waveguides*. 2006, Elsevier. p. 13-55.
68. A. Dhakal, P. Wuytens, F. Peyskens, A. Subramanian, A. Skirtach, N. Le Thomas, and R. Baets. *Nanophotonic lab-on-a-chip Raman sensors: A sensitivity comparison with confocal Raman microscope*. in *2015 International Conference on BioPhotonics (BioPhotonics)*. 2015.
69. J. Michon, D. Kita, and J. Hu, *Sensitivity comparison of free-space and waveguide Raman for bulk sensing.* Journal of the Optical Society of America B, 2020. **37**(7): p. 2012-2020.
70. G.E. Walrafen and J. Stone, *Intensification of Spontaneous Raman Spectra by Use of Liquid Core Optical Fibers.* Applied Spectroscopy, 1972. **26**(6): p. 585-589.
71. Y. Levy, C. Imbert, J. Cipriani, S. Racine, and R. Dupeyrat, *Raman scattering of thin films as a waveguide.* Optics Communications, 1974. **11**(1): p. 66-69.
72. J.F. Rabolt, R. Santo, and J.D. Swalen, *Raman Spectroscopy of Thin Polymer Films Using Integrated Optical Techniques.* Applied Spectroscopy, 1979. **33**(6): p. 549-551.
73. J.F. Rabolt, R. Santo, N.E. Schlotter, and J.D. Swalen, *Integrated Optics and Raman Scattering: Molecular Orientation in Thin Polymer Films and Langmuir-Blodgett Monolayers.* IBM Journal of Research and Development, 1982. **26**(2): p. 209-216.
74. N.E. Schlotter and J.F. Rabolt, *Raman spectroscopy in polymeric thin film optical waveguides. 1. Polarized measurements and orientational effects in two-dimensional films.* The Journal of Physical Chemistry, 1984. **88**(10): p. 2062-2067.
75. J.S. Kanger, C. Otto, and J. Greve, *Stimulated Raman Gain Spectroscopy of Thin Layers Using Dielectric Waveguides.* The Journal of Physical Chemistry, 1996. **100**(40): p. 16293-16297.

76. A. Dhakal, A.Z. Subramanian, P. Wuytens, F. Peyskens, N. Le Thomas, and R. Baets, *Evanescent excitation and collection of spontaneous Raman spectra using silicon nitride nanophotonic waveguides.* Optics Letters, 2014. **39**(13): p. 4025.
77. E. Le Ru and P. Etchegoin, *Principles of Surface-Enhanced Raman Spectroscopy and related plasmonic effects*. 2008: Elsevier.
78. D.M. Kita, J. Michon, S.G. Johnson, and J. Hu, *Are slot and sub-wavelength grating waveguides better than strip waveguides for sensing?* Optica, 2018. **5**(9): p. 1046.
79. C.C. Evans, C. Liu, and J. Suntivich, *TiO_2 Nanophotonic Sensors for Efficient Integrated Evanescent Raman Spectroscopy.* ACS Photonics, 2016. **3**(9): p. 1662-1669.
80. N. Le Thomas, Z. Liu, C. Lin, H. Zhao, and R. Baets, *Raman on-chip: current status and future tracks*. SPIE OPTO. Vol. 11689. 2021: SPIE.
81. D.A. Long, *The Raman effect: a unified treatment of the theory of Raman scattering by molecules*. 2002: John Wiley & Sons.
82. Y. Zhao, M. Jenkins, P. Measor, K. Leake, S. Liu, H. Schmidt, and A.R. Hawkins, *Hollow waveguides with low intrinsic photoluminescence fabricated with Ta_2O_5 and SiO_2 films.* Applied Physics Letters, 2011. **98**(9): p. 091104.
83. D. Tuschel, *Selecting an excitation wavelength for Raman spectroscopy.* Spectroscopy, 2016. **31**: p. 14–23.
84. Y.-K. Min, T. Yamamoto, E. Kohda, T. Ito, and H.-o. Hamaguchi, *1064 nm near-infrared multichannel Raman spectroscopy of fresh human lung tissues.* Journal of Raman Spectroscopy, 2005. **36**(1): p. 73-76.
85. C.A. Lieber, H. Wu, and W. Yang, *Tissue measurement using 1064 nm dispersive Raman spectroscopy*, in *Advanced Biomedical and Clinical Diagnostic Systems XI*. 2013, SPIE.
86. M.W. Meyer, J.S. Lupoi, and E.A. Smith, *1064nm dispersive multichannel Raman spectroscopy for the analysis of plant lignin.* Analytica Chimica Acta, 2011. **706**(1): p. 164-170.
87. A. Dhakal, A. Raza, F. Peyskens, A.Z. Subramanian, S. Clemmen, N. Le Thomas, and R. Baets, *Efficiency of evanescent excitation and collection of spontaneous Raman scattering near high index contrast channel waveguides.* Optics Express, 2015. **23**(21): p. 27391.
88. N. Le Thomas, A. Dhakal, A. Raza, F. Peyskens, and R. Baets, *Impact of fundamental thermodynamic fluctuations on light propagating in photonic waveguides made of amorphous materials.* Optica, 2018. **5**(4): p. 328-336.
89. A. Raza, S. Clemmen, P. Wuytens, M. de Goede, A.S.K. Tong, N. Le Thomas, C. Liu, J. Suntivich, A.G. Skirtach, S.M. Garcia-Blanco, D.J. Blumenthal, J.S. Wilkinson, and R. Baets, *High index contrast photonic platforms for on-chip Raman spectroscopy.* Optics Express, 2019. **27**(16): p. 23067.
90. T. Tsuchiya, H. Imai, S. Miyoshi, P.-A. Glans, J. Guo, and S. Yamaguchi, *X-Ray absorption, photoemission spectroscopy, and Raman scattering analysis of amorphous tantalum oxide with a large extent of oxygen nonstoichiometry.* Physical Chemistry Chemical Physics, 2011. **13**(38): p. 17013.
91. A. Dhakal, P. Wuytens, A. Raza, N. Le Thomas, and R. Baets, *Silicon Nitride Background in Nanophotonic Waveguide Enhanced Raman Spectroscopy.* Materials, 2017. **10**(2): p. 140.
92. W. Lee, P. Muñoz-Galindo, I. Hegeman, Y.-S. Yong, M. Dijkstra, S.M. García-Blanco, and H.L. Offerhaus, *Study on multiple waveguide platforms for waveguide integrated Raman spectroscopy.* OSA Continuum, 2020. **3**(5): p. 1322-1333.
93. A. Pope, A. Schulte, Y. Guo, L.K. Ono, B.R. Cuenya, C. Lopez, K. Richardson, K. Kitanovski, and T. Winningham, *Chalcogenide waveguide structures as substrates and guiding layers for evanescent wave Raman spectroscopy of bacteriorhodopsin.* Vibrational Spectroscopy, 2006. **42**(2): p. 249-253.

94. A. Dhakal, F. Peyskens, S. Clemmen, A. Raza, P. Wuytens, H. Zhao, N. Le Thomas, and R. Baets, *Single mode waveguide platform for spontaneous and surface-enhanced on-chip Raman spectroscopy.* Interface focus, 2016. **6**(4): p. 20160015.
95. O. Tagit and N. Hildebrandt, *Fluorescence Sensing of Circulating Diagnostic Biomarkers Using Molecular Probes and Nanoparticles.* ACS Sensors, 2017. **2**(1): p. 31-45.
96. Y. Chu, Y. Gao, W. Tang, L. Qiang, Y. Han, J. Gao, Y. Zhang, H. Liu, and L. Han, *Attomolar-Level Ultrasensitive and Multiplex microRNA Detection Enabled by a Nanomaterial Locally Assembled Microfluidic Biochip for Cancer Diagnosis.* Analytical Chemistry, 2021. **93**(12): p. 5129-5136.
97. A. Qu, X. Wu, L. Xu, L. Liu, W. Ma, H. Kuang, and C. Xu, *SERS- and luminescence-active Au–Au–UCNP trimers for attomolar detection of two cancer biomarkers.* Nanoscale, 2017. **9**(11): p. 3865-3872.
98. J.U. Lee, W.H. Kim, H.S. Lee, K.H. Park, and S.J. Sim, *Quantitative and specific detection of exosomal miRNAs for accurate diagnosis of breast cancer using a surface-enhanced Raman scattering sensor based on plasmonic head-flocked gold nanopillars.* Small, 2019. **15**(17): p. 1804968.
99. M.C. Estevez, M. Alvarez, and L.M. Lechuga, *Integrated optical devices for lab-on-a-chip biosensing applications.* Laser & Photonics Reviews, 2011. **6**(4): p. 463-487.
100. M.-J. Bañuls, R. Puchades, and Á. Maquieira, *Chemical surface modifications for the development of silicon-based label-free integrated optical (IO) biosensors: A review.* Analytica Chimica Acta, 2013. **777**: p. 1-16.
101. M. Rabe, D. Verdes, and S. Seeger, *Understanding protein adsorption phenomena at solid surfaces.* Advances in Colloid and Interface Science, 2011. **162**(1-2): p. 87-106.
102. Z. Altintas, Y. Uludag, Y. Gurbuz, and I. Tothill, *Development of surface chemistry for surface plasmon resonance based sensors for the detection of proteins and DNA molecules.* Analytica Chimica Acta, 2012. **712**: p. 138-144.
103. J.J. Gooding and S. Ciampi, *The molecular level modification of surfaces: from self-assembled monolayers to complex molecular assemblies.* Chemical Society Reviews, 2011. **40**(5): p. 2704.
104. A. Sassolas, L.J. Blum, and B.D. Leca-Bouvier, *Immobilization strategies to develop enzymatic biosensors.* Biotechnology Advances, 2012. **30**(3): p. 489-511.
105. P. Jonkheijm, D. Weinrich, H. Schröder, C.M. Niemeyer, and H. Waldmann, *Chemical Strategies for Generating Protein Biochips.* Angewandte Chemie International Edition, 2008. **47**(50): p. 9618-9647.
106. C. Adessi, *Solid phase DNA amplification: characterisation of primer attachment and amplification mechanisms.* Nucleic Acids Research, 2000. **28**(20): p. 87e-87.
107. V. Leiro, P. Parreira, S.C. Freitas, M.C.L. Martins, and A.P. Pêgo, *Conjugation Chemistry Principles and Surface Functionalization of Nanomaterials*, in *Biomedical Applications of Functionalized Nanomaterials*. 2018, Elsevier. p. 35-66.
108. G.T. Hermanson, *The Reactions of Bioconjugation*, in *Bioconjugate Techniques*. 2013, Elsevier. p. 229-258.
109. M. Chockalingam, A. Magenau, S.G. Parker, M. Parviz, S.R.C. Vivekchand, K. Gaus, and J.J. Gooding, *Biointerfaces on Indium–Tin Oxide Prepared from Organophosphonic Acid Self-Assembled Monolayers.* Langmuir, 2014. **30**(28): p. 8509-8515.
110. R.P. Gandhiraman, V. Gubala, L.C.H. Nam, C. Volcke, C. Doyle, B. James, S. Daniels, and D.E. Williams, *Deposition of chemically reactive and repellent sites on biosensor chips for reduced non-specific binding.* Colloids and Surfaces B: Biointerfaces, 2010. **79**(1): p. 270-275.
111. C. Gruian, A. Vulpoi, E. Vanea, B. Oprea, H.J. Steinhoff, and S. Simon, *The Attachment Affinity of Hemoglobin toward Silver-Containing Bioactive Glass Functionalized with Glutaraldehyde.* The Journal of Physical Chemistry B, 2013. **117**(51): p. 16558-16564.

112. A.B. González-Guerrero, J. Maldonado, S. Herranz, and L.M. Lechuga, *Trends in photonic lab-on-chip interferometric biosensors for point-of-care diagnostics.* Analytical Methods, 2016. **8**(48): p. 8380-8394.
113. C. Mas-Moruno, B. Garrido, D. Rodriguez, E. Ruperez, and F.J. Gil, *Biofunctionalization strategies on tantalum-based materials for osseointegrative applications.* Journal of Materials Science: Materials in Medicine, 2015. **26**(2).
114. M. Kutscher, M. Rosenberger, B. Schmauss, L. Meinel, U. Lorenz, K. Ohlsen, R. Hellmann, and O. Germershaus, *Surface functionalization allowing repetitive use of optical sensors for real-time detection of antibody-bacteria interaction.* Journal of Biophotonics, 2015. **9**(7): p. 730-737.
115. A. Ramachandran, S. Wang, J. Clarke, S.J. Ja, D. Goad, L. Wald, E.M. Flood, E. Knobbe, J.V. Hryniewicz, S.T. Chu, D. Gill, W. Chen, O. King, and B.E. Little, *A universal biosensing platform based on optical micro-ring resonators.* Biosensors and Bioelectronics, 2008. **23**(7): p. 939-944.
116. J. Escorihuela, M.-J. Bañuls, R. Puchades, and Á. Maquieira, *Development of Oligonucleotide Microarrays onto Si-Based Surfaces via Thioether Linkage Mediated by UV Irradiation.* Bioconjugate Chemistry, 2012. **23**(10): p. 2121-2128.
117. C. Mateo, R. Torres, G. Fernández-Lorente, C. Ortiz, M. Fuentes, A. Hidalgo, F. López-Gallego, O. Abian, J.M. Palomo, L. Betancor, B.C.C. Pessela, J.M. Guisan, and R. Fernández-Lafuente, *Epoxy-Amino Groups: A New Tool for Improved Immobilization of Proteins by the Epoxy Method.* Biomacromolecules, 2003. **4**(3): p. 772-777.
118. G.Y. Wiederschain, *The Molecular Probes handbook. A guide to fluorescent probes and labeling technologies*. 2011: Springer Nature BV.
119. G.T. Hermanson, *Bioconjugate techniques*. 2013: Academic press.
120. D. Duval and L.M. Lechuga, *Optical Waveguide Biosensors*, in *Photonics*. 2015, Wiley. p. 323-365.
121. G.C. Hoops, *Effects of sodium chloride on the properties of chlorophyll submonolayer adsorbed onto hydrophobic and hydrophilic surfaces using broadband spectroscopy with single-mode integrated optical waveguides.* Optical Engineering, 2011. **50**(7): p. 071109.
122. S.R. Makhsin, P. Gardner, N.J. Goddard, and P.J. Scully, *Surface modification of titanium-coated glass substrate embedded acrylate-based hydrogel film for optical metal clad leaky waveguide (MCLW) biosensors*, in *2017 IEEE SENSORS*. 2017, IEEE.
123. K. Schmitt, K. Oehse, G. Sulz, and C. Hoffmann, *Evanescent field Sensors Based on Tantalum Pentoxide Waveguides – A Review.* Sensors, 2008. **8**(2): p. 711-738.
124. S.P. Pujari, L. Scheres, A.T.M. Marcelis, and H. Zuilhof, *Covalent Surface Modification of Oxide Surfaces.* Angewandte Chemie International Edition, 2014. **53**(25): p. 6322-6356.
125. H. Mukundan, H. Xie, A.S. Anderson, W.K. Grace, J.E. Shively, and B.I. Swanson, *Optimizing a Waveguide-Based Sandwich Immunoassay for Tumor Biomarkers: Evaluating Fluorescent Labels and Functional Surfaces.* Bioconjugate Chemistry, 2009. **20**(2): p. 222-230.
126. H. Mukundan, J.Z. Kubicek, A. Holt, J.E. Shively, J.S. Martinez, K. Grace, W.K. Grace, and B.I. Swanson, *Planar optical waveguide-based biosensor for the quantitative detection of tumor markers.* Sensors and Actuators B: Chemical, 2009. **138**(2): p. 453-460.
127. H. Mukundan, S. Kumar, D.N. Price, S.M. Ray, Y.-J. Lee, S. Min, S. Eum, J. Kubicek-Sutherland, J.M. Resnick, W.K. Grace, A.S. Anderson, S.H. Hwang, S.N. Cho, L.E. Via, C. Barry, R. Sakamuri, and B.I. Swanson, *Rapid detection of Mycobacterium tuberculosis biomarkers in a sandwich immunoassay format using a waveguide-based optical biosensor.* Tuberculosis, 2012. **92**(5): p. 407-416.
128. A.S. Anderson, A.M. Dattelbaum, G.A. Montaño, D.N. Price, J.G. Schmidt, J.S. Martinez, W.K. Grace, K.M. Grace, and B.I. Swanson, *Functional PEG-Modified Thin Films for Biological Detection.* Langmuir, 2008. **24**(5): p. 2240-2247.

129. P. Kozma, A. Hámori, S. Kurunczi, K. Cottier, and R. Horvath, *Grating coupled optical waveguide interferometer for label-free biosensing.* Sensors and Actuators B: Chemical, 2011. **155**(2): p. 446-450.
130. Y. Xin, G. Pandraud, L. Otten, Y. Zhang, and P. French, *Surface Functionalization of SU-8 Vertical Waveguide for Biomedical Sensing: Bacteria Diagnosis.* Proceedings, 2018. **2**(13): p. 1081.
131. R. Boissezon, J. Muller, V. Beaugeard, S. Monge, and J.-J. Robin, *Organophosphonates as anchoring agents onto metal oxide-based materials: synthesis and applications.* RSC Advances, 2014. **4**(67): p. 35690.
132. P. Canepa, G. Gonella, G. Pinto, V. Grachev, M. Canepa, and O. Cavalleri, *Anchoring of Aminophosphonates on Titanium Oxide for Biomolecular Coupling.* The Journal of Physical Chemistry C, 2019. **123**(27): p. 16843-16850.
133. A. Muriano, K.N.A. Thayil, J.P. Salvador, P. Loza-Alvarez, S. Soria, R. Galve, and M.P. Marco, *Two-photon fluorescent immunosensor for androgenic hormones using resonant grating waveguide structures.* Sensors and Actuators B: Chemical, 2012. **174**: p. 394-401.
134. X. Han, X. Sun, T. He, and S. Sun, *Formation of Highly Stable Self-Assembled Alkyl Phosphonic Acid Monolayers for the Functionalization of Titanium Surfaces and Protein Patterning.* Langmuir, 2014. **31**(1): p. 140-148.
135. G. Rong, A. Najmaie, J.E. Sipe, and S.M. Weiss, *Nanoscale porous silicon waveguide for label-free DNA sensing.* Biosensors and Bioelectronics, 2008. **23**(10): p. 1572-1576.
136. S.C.B. Gopinath, K. Awazu, and M. Fujimaki, *Waveguide-Mode Sensors as Aptasensors.* Sensors, 2012. **12**(2): p. 2136-2151.
137. A. Al-Jawdah, A. Nabok, H. Abu-Ali, G. Catanante, J.-L. Marty, and A. Szekacs, *Highly sensitive label-free in vitro detection of aflatoxin B1 in an aptamer assay using optical planar waveguide operating as a polarization interferometer.* Analytical and Bioanalytical Chemistry, 2019. **411**(29): p. 7717-7724.
138. N.F. Tyndall, T.H. Stievater, D.A. Kozak, K. Koo, R.A. McGill, M.W. Pruessner, W.S. Rabinovich, and S.A. Holmstrom, *Waveguide-enhanced Raman spectroscopy of trace chemical warfare agent simulants.* Optics Letters, 2018. **43**(19): p. 4803.
139. J. Veerbeek and J. Huskens, *Applications of Monolayer-Functionalized H-Terminated Silicon Surfaces: A Review.* Small Methods, 2017. **1**(4): p. 1700072.
140. H. Qiao, B. Guan, J.J. Gooding, and P.J. Reece, *Protease detection using a porous silicon based Bloch surface wave optical biosensor.* Optics Express, 2010. **18**(14): p. 15174.
141. H. Qiao, A.H. Soeriyadi, B. Guan, P.J. Reece, and J.J. Gooding, *The analytical performance of a porous silicon Bloch surface wave biosensors as protease biosensor.* Sensors and Actuators B: Chemical, 2015. **211**: p. 469-475.
142. L. De Stefano, P. Arcari, A. Lamberti, C. Sanges, L. Rotiroti, I. Rea, and I. Rendina, *DNA Optical Detection Based on Porous Silicon Technology: from Biosensors to Biochips.* Sensors, 2007. **7**(2): p. 214-221.
143. M.-J. Bañuls, V. González-Pedro, C.A. Barrios, R. Puchades, and Á. Maquieira, *Selective chemical modification of silicon nitride/silicon oxide nanostructures to develop label-free biosensors.* Biosensors and Bioelectronics, 2010. **25**(6): p. 1460-1466.
144. M. Cerruti, S. Fissolo, C. Carraro, C. Ricciardi, A. Majumdar, and R. Maboudian, *Poly(ethylene glycol) Monolayer Formation and Stability on Gold and Silicon Nitride Substrates.* Langmuir, 2008. **24**(19): p. 10646-10653.
145. P. Wu, P. Hogrebe, and D.W. Grainger, *DNA and protein microarray printing on silicon nitride waveguide surfaces.* Biosensors and Bioelectronics, 2006. **21**(7): p. 1252-1263.
146. N.-P. Huang, J. Vörös, S.M. De Paul, M. Textor, and N.D. Spencer, *Biotin-Derivatized Poly(l-lysine)-g-poly(ethylene glycol): A Novel Polymeric Interface for Bioaffinity Sensing.* Langmuir, 2002. **18**(1): p. 220-230.

147. J. Vörös, J.J. Ramsden, G. Csúcs, I. Szendrő, S.M. De Paul, M. Textor, and N.D. Spencer, *Optical grating coupler biosensors.* Biomaterials, 2002. **23**(17): p. 3699-3710.
148. H.M. Grandin, B. Städler, M. Textor, and J. Vörös, *Waveguide excitation fluorescence microscopy: A new tool for sensing and imaging the biointerface.* Biosensors and Bioelectronics, 2006. **21**(8): p. 1476-1482.
149. B. Agnarsson, A. Lundgren, A. Gunnarsson, M. Rabe, A. Kunze, M. Mapar, L. Simonsson, M. Bally, V.P. Zhdanov, and F. Höök, *Evanescent Light-Scattering Microscopy for Label-Free Interfacial Imaging: From Single Sub-100 nm Vesicles to Live Cells.* ACS Nano, 2015. **9**(12): p. 11849-11862.
150. J. Satija, V.V.R. Sai, and S. Mukherji, *Dendrimers in biosensors: Concept and applications.* Journal of Materials Chemistry, 2011. **21**(38): p. 14367.
151. F. Vollmer, S. Arnold, D. Braun, I. Teraoka, and A. Libchaber, *Multiplexed DNA Quantification by Spectroscopic Shift of Two Microsphere Cavities.* Biophysical Journal, 2003. **85**(3): p. 1974-1979.
152. J. Adrian, S. Pasche, J.-M. Diserens, F. Sánchez-Baeza, H. Gao, M.P. Marco, and G. Voirin, *Waveguide interrogated optical immunosensor (WIOS) for detection of sulfonamide antibiotics in milk.* Biosensors and Bioelectronics, 2009. **24**(11): p. 3340-3346.
153. Z. Wang, M.N. Zervas, P.N. Bartlett, and J.S. Wilkinson, *Surface and waveguide collection of Raman emission in waveguide-enhanced Raman spectroscopy.* Optics Letters, 2016. **41**(17): p. 4146.
154. D.M. Kita, J. Michon, and J. Hu, *A packaged, fiber-coupled waveguide-enhanced Raman spectroscopic sensor.* Optics Express, 2020. **28**(10): p. 14963.
155. X. Nie, N. Turk, Y. Li, Z. Liu, and R. Baets, *High extinction ratio on-chip pump-rejection filter based on cascaded grating-assisted contra-directional couplers in silicon nitride rib waveguides.* Optics Letters, 2019. **44**(9): p. 2310-2313.
156. K. Reynkens, S. Clemmen, A. Raza, H. Zhao, J.S.-D. Peñaranda, C. Detavernier, and R. Baets, *Mitigation of photon background in nanoplasmonic all-on-chip Raman sensors.* Optics Express, 2020. **28**(22): p. 33564-33572.
157. N.F. Tyndall, T.H. Stievater, D.A. Kozak, M.W. Pruessner, and W.S. Rabinovich, *Passive photonic integration of lattice filters for waveguide-enhanced Raman spectroscopy.* Optics Express, 2020. **28**(23): p. 34927-34934.
158. K. Kasaya, O. Mitomi, M. Naganuma, Y. Kondo, and Y. Noguchi, *A simple laterally tapered waveguide for low-loss coupling to single-mode fibers.* IEEE Photonics Technology Letters, 1993. **5**(3): p. 345-347.
159. N. Hatori, T. Shimizu, M. Okano, M. Ishizaka, T. Yamamoto, Y. Urino, M. Mori, T. Nakamura, and Y. Arakawa, *A Hybrid Integrated Light Source on a Silicon Platform Using a Trident Spot-Size Converter.* Journal of Lightwave Technology, 2014. **32**(7): p. 1329-1336.
160. M.A. Ettabib, Z. Liu, M.N. Zervas, and J.S. Wilkinson, *Optimized design for grating-coupled waveguide-enhanced Raman spectroscopy.* Optics Express, 2020. **28**(25): p. 37226-37235.
161. R. Marchetti, C. Lacava, L. Carroll, K. Gradkowski, and P. Minzioni, *Coupling strategies for silicon photonics integrated chips [Invited].* Photonics Research, 2019. **7**(2): p. 201.

For TOC only

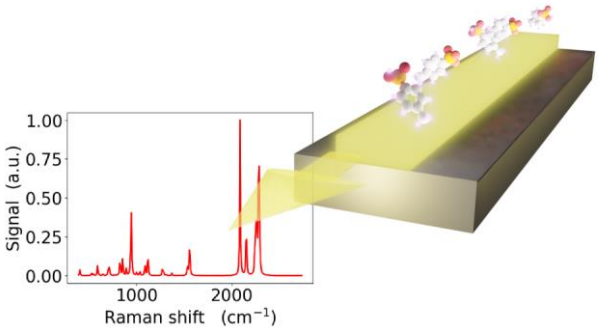

For TOC only